Journal of Asian Earth Sciences 134 (2017) 330–351

Contents lists available at ScienceDirect

Journal of Asian Earth Sciences

journal homepage: www.elsevier.com/locate/jseaes

Full length Article

Isotopic (U-Pb, Nd) and geochemical constraints on the origins of the Aileu and Gondwana sequences of Timor

S.D. Boger *, L.G. Spelbrink, R.I. Lee, M. Sandiford, R. Maas, J.D. Woodhead

School of Earth Sciences, The University of Melbourne, Victoria 3010, Australia

ARTICLE INFO

Article history:
Received 3 August 2016
Received in revised form 23 November 2016
Accepted 23 November 2016
Available online 24 November 2016

Keywords:
Timor Léste
Banda Arc
Tectonics
Zircon geochronology
Nd-isotopes
Geochemistry
Sediment provenance

ABSTRACT

Detrital zircon U-Pb age data collected from the argillitic sedimentary rocks of the Timorese Aileu Complex and Gondwana Sequence indicate that both units were derived from a common source containing 200–600 Ma, 900–1250 Ma and 1450–1900 Ma zircon. The modally most significant age population within this range of ages dates to c. 260 Ma. The observed spectrum of ages can be traced to the eastern active margin of Pangaea and its immediate foreland, which today is best exposed along the northeast coast of Australia. Compared to the relative homogeneity of the detrital zircon age data, geochemical and Nd isotopic data show that the mudstones of the Aileu Complex are on average more siliceous, have higher K_2O/Na_2O, Rb/Sr, Th/Sc and yield notably older Nd T_{DM} model ages when compared to those from the Gondwana Sequence. These data are interpreted to suggest that, although both sequences share a common east Pangaea provenance, they were eroded from different sections of this active margin and deposited in spatially separated basins. The present proximity of these units is a result of their tectonic juxtaposition during the Pliocene to Recent collision between the northern edge of the Indo–Australia plate and the Banda Arc.

Crown Copyright © 2016 Published by Elsevier Ltd. All rights reserved.

1. Introduction

The rapid northwards drift of the Australian plate since the middle Eocene (c. 45 Ma) has been accommodated via the northwards subduction of Indo-Australian oceanic crust beneath the southern margin of Sundaland (Cande and Mutter, 1982; Hall, 2002; Hall, 2012). Plate convergence at this margin was accommodated firstly by the formation of the Sunda Arc, then, from the end of the Oligocene (c. 25 Ma), by the development of the Banda Arc (Fig. 1). The Banda Arc formed in response to arc-continent collision between the Sula Spur, the northernmost continental promontory of the Indo-Australian plate, and the southern margin of Sundaland. As a consequence of this collision the subducted Indo-Australian oceanic crust tore and, west of the Sula Spur, slab roll back resulted in the south and eastward migration of the proto-Banda Arc into the Banda embayment (Hall, 2012; Spakman and Hall, 2010).

The southward migration of the Banda Arc together with the ongoing northwards movement of the Indo-Australian plate culminated at approximately 4 Ma in a second phase of arc-continent collision. This event was centred on the island of Timor and is recorded in the geology of the island via the complex intercalation of autochthonous sedimentary rocks derived from the northern margin of the Indo-Australian plate and allochthonous rocks derived from the pre-collision Banda Arc (Abbott and Chamalaun, 1981; Audley-Charles, 2004, 2011). Collision also transferred the Banda Arc islands of Wetar and Alor to the Indo-Australian plate, with most present day convergence now accommodated along the south-dipping Wetar Thrust (Genrich et al., 1996; Nugroho et al., 2009; Koulali et al., 2016).

In addition to rocks with affinities to the pre-collisional Indo-Australian plate and the Banda Arc, the geology of Timor also includes a sequence of meta-sedimentary and meta-igneous rocks that preserve facets common to both the autochthonous Indo–Australian margin and the allochthonous Banda Arc (Fig. 1). Known as the Aileu Complex and exposed over a broad area along the north coast of Timor, the ambiguous origin of these rocks has seen them attributed to both plates (e.g. Audley-Charles, 1968; Carter et al., 1976; Barber et al., 1977; Harris, 1991; Charlton et al., 2002; Keep and Haig, 2010; Ely et al., 2014).

To address the origin of both the Aileu Complex and the sedimentary rocks of the Indo-Australian margin, this contribution presents two new datasets. The first is a whole rock, trace and rare earth element geochemical and Nd isotopic dataset obtained from argillitic sediments collected from both the Aileu Complex and the Indo–Australian Gondwana Sequence. The second is a detrital

* Corresponding author.
E-mail address: sdboger@unimelb.edu.au (S.D. Boger).

http://dx.doi.org/10.1016/j.jseaes.2016.11.026
1367-9120/Crown Copyright © 2016 Published by Elsevier Ltd. All rights reserved.

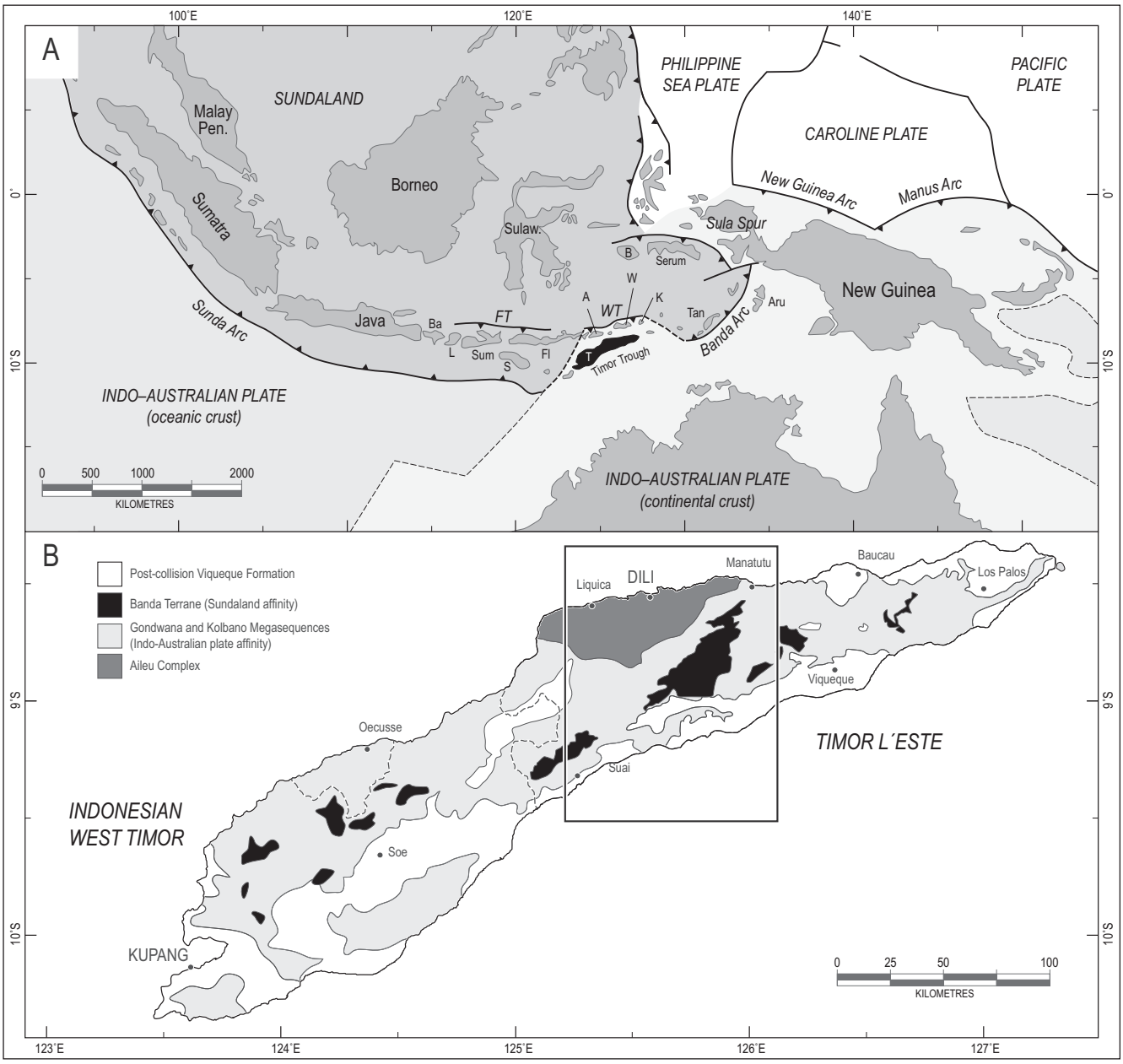

Fig. 1. Tectonic setting and regional geology of northern Australia and southeast Asia. (A) Configuration of the tectonic plates surrounding Timor. Plate boundaries are after Hall (2002), Simons et al. (2007), Nugroho et al. (2009) and Špičák et al. (2013). Abbreviated island names are: A = Alor, B = Buru, Ba = Bali, Fl = Flores, K = Kisar, L = Lombok, S = Sumba, Sum = Sumbawa, Tan = Tanimbar and W = Wetar. Timor (T) is highlighted in black. FT = Flores Thrust, WT = Wetar Thrust. (B) Simplified regional geology of Timor. Unit boundaries after Audley-Charles (1968) and Charlton (2002) and the mapping undertaken as part of this study. Boxed area is the study area, which is enlarged in Fig. 2.

zircon age dataset collected from two sandstone samples from the Gondwana Sequence. The former of these datasets represents the first geochemical and Nd isotopic data collected from the sedimentary rocks of Timor, while the latter builds on the recently collected detrital zircon datasets of Harris (2006), Ely et al. (2014), Kwon et al. (2014), Spencer et al. (2016) and Zimmermann and Hall (2016).

Although weathering and sedimentary sorting do play a role in modifying the composition of the sedimentary detritus (McLennan et al., 1993), detrital zircon, geochemical, and Nd isotopic methods are proven tools for sediment provenance (Bhatia, 1983; Dickinson et al., 1983; Bhatia and Crook, 1986; Roser and Korsch, 1986; McLennan et al., 1990; McLennan and Taylor, 1991; Verma and Armstrong-Altrin, 2013). Zircon is extremely resistant to both chemical weathering and thermal resetting, while trace elements such as Th, Zr, Hf, Nb, Ti and Sc, the rare earth elements, and the Sm-Nd isotopic system, are good tectonic tracers given their limited mobility in sedimentary processes and their short residence time in seawater (Taylor and McLennan, 1985). Collectively the data presented allows for a more informed discussion of the likely origin of the Aileu Complex and its relationship to the other geologic components of Timor.

2. Regional geology

On Timor the pre-collision margin of the Indo-Australian plate (Fig. 1) is defined by the early Permian to middle Jurassic Gondwana Sequence (300–190 Ma) and the Cretaceous to middle Miocene Kolbano Sequence (115–15 Ma). The Gondwana Sequence

was deposited near the northeastern edge of Pangaea and is composed of a thick sequence of terrigenous and chemical sediment that, for the present study, is taken to include the Atahoc, Cribas, Niof, Aitutu, Babulu and Wai Luli formations. The Maubisse Formation, which is commonly regarded as the lowermost part of the Gondwana Sequence (e.g. Charlton et al., 2002), is excluded given it: (i) is intercalated with the mudstones of the Aileu Complex and, (ii) is separated from the remainder of the Gondwana Sequence by the Laclo Fault (Fig. 2), a structure we consider to record significant tectonic displacement.

The oldest exposed components of the Gondwana Sequence are thus taken as the early Permian Atahoc and Cribas formations, units composed mostly of finely laminated mudstone and shale (Charlton et al., 2002). The Atahoc Formation is comprised mostly of well-lithified black shale and separated from the Cribas Formation by a layer of amygdaloidal basalt (Audley-Charles, 1968). The bulk of the Cribas Formation is composed of shale with common calcareous and clay-ironstone nodules. Bedded limestone and thickly bedded sandstone become more common toward the top of this sequence (Charlton et al., 2002).

The late Permian to early Triassic Niof Formation is the oldest component of the Triassic in Timor (Charlton et al., 2002, 2009). It is not definitively known in East Timor, but described from the Kekneno area of West Timor (Bird and Cook, 1991). It is comprised of dark grey shale interbedded with minor siltstone, sandstone and phosphate nodule horizons. Toward the top of this sequence thin shelly limestone is also present (Charlton et al., 2009). The Niof Formation is in turn succeeded by the Aitutu and Babulu Formations. These two formations are thought to have been deposited contemporaneously from the middle Triassic until the earliest Jurassic. The Aitutu Formation is comprised of dark grey, pale-weathering limestone, bedded at the centimetre and decimetre scale, and intercalated with dark grey calcareous shale. The Babulu Formation is a dominantly siliciclastic succession comprised of

SAMPLE	LATITUDE	LONGITUDE
AILEU COMPLEX		
LSP013	8.5273°S	125.6467°E
LSP076	8.6207°S	125.8074°E
LSP084	8.4797°S	125.8628°E
LSP099	8.5632°S	125.4855°E
LSP102	8.5479°S	125.7293°E
RIL031	8.6917°S	125.5478°E
RIL047	8.7963°S	125.5670°E
RIL061	8.6107°S	125.6307°E
RIL067	8.6128°S	125.5301°E
RIL075	8.7128°S	125.6395°E
RIL077	8.6916°S	125.6504°E
RIL169	8.7584°S	125.5806°E
RIL196	8.7466°S	125.6501°E
RIL228	8.7607°S	125.4885°E
TKI036	8.8426°S	125.5353°E
TKI066	8.4954°S	125.8817°E

SAMPLE	LATITUDE	LONGITUDE
GONDWANA SEQUENCE		
LSP077	8.6115°S	125.8322°E
LSP078	8.5173°S	125.9872°E
LSP079	8.5502°S	125.9343°E
LSP111	8.8579°S	125.5843°E
LSP118	8.7072°S	125.7804°E
LSP122	8.7084°S	125.7364°E
LSP141	8.5692°S	125.8226°E
OLI040	8.6917°S	125.8600°E
OLI041	8.6444°S	125.9811°E
OLI052	8.5889°S	125.9038°E
RIL024	8.8630°S	125.4247°E
RIL029	8.9161°S	125.4239°E
RIL181	8.5153°S	125.8789°E

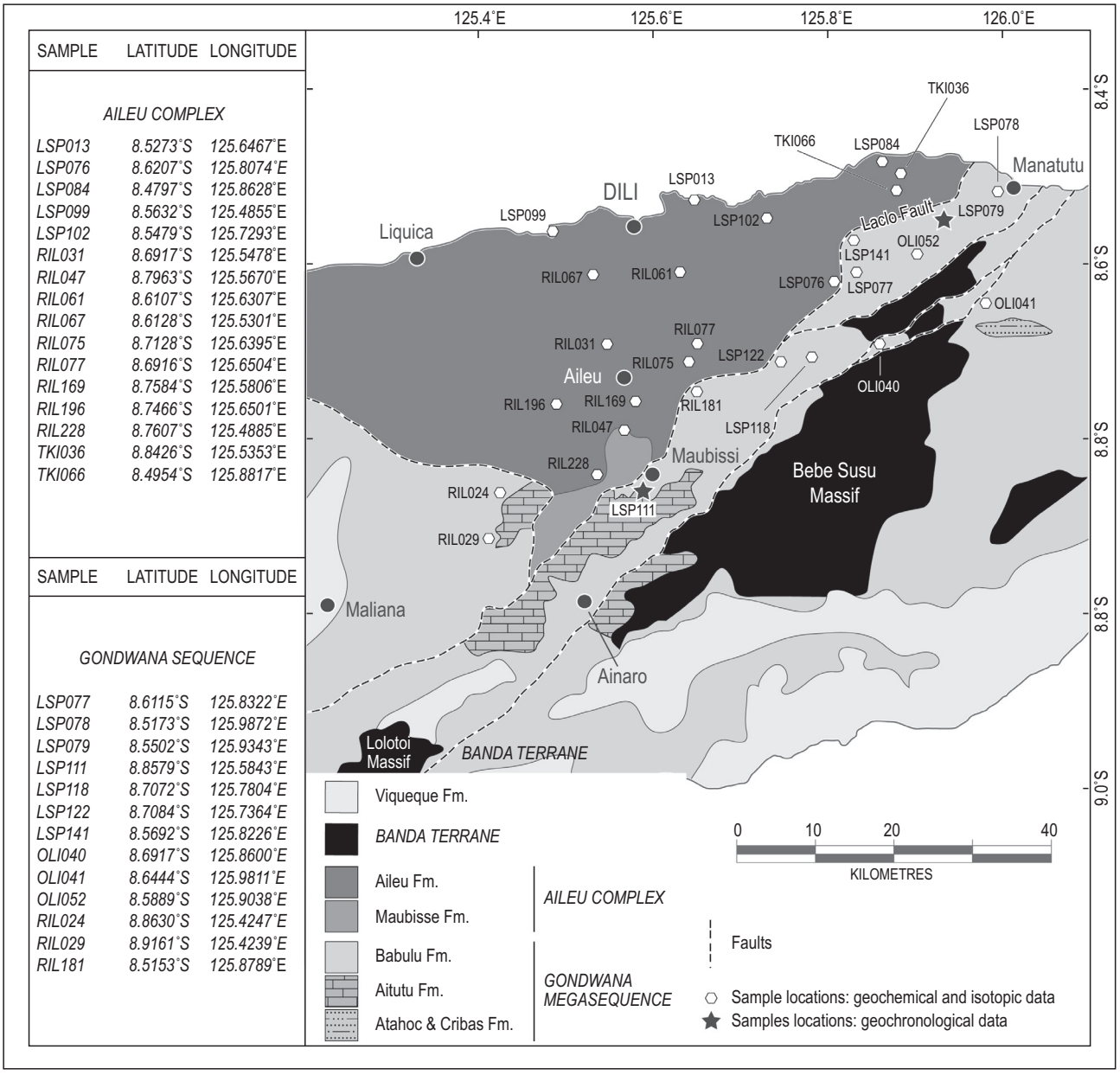

Fig. 2. The area of study in north-central Timor Léste. Figure illustrates the main tectonic units and the distribution of sample locations. Coordinates of sample locations (datum: WGS84) are given in the table left.

greenish to yellow-brown siltstone and sandstone, with lesser red siltstone and bituminous shale with local intercalations of marl and limestone (Charlton et al., 2009). Compositional layering is mostly developed on the scale of several centimetres to several metres. The youngest component of the Gondwana Sequence is the early to middle Jurassic Wai Luli Formation. It is comprised of medium grey, red and green mudstone and marl, interbedded with thin layers of limestone (Charlton et al., 2009).

The overlying Kolbano Sequence is defined mostly by deep marine limestone, shale and radiolarites that were deposited on the north Australian passive margin after the rifting and separation of the Argo and Banda (or greater Sula Spur) blocks (Charlton and Wall, 1994; Charlton, 2001; Haig and McCartain, 2007; Hall, 2012). These blocks separated from the northeast margin of Gondwana in the late Jurassic and are now found in southwest Borneo and parts of Java and Sulawesi (Hall, 2012; Metcalfe, 2013b). Both the Gondwana and Kolbano sequences record diagenetic to lower anchizonal grade metamorphism (Harris et al., 2000), conditions that reflect either their pre-collisional burial history, or their subtle thermal reworking as a result of orogenesis.

In contrast to the Gondwana Sequence, the Banda Terrane (Fig. 1) is defined by a metamorphic basement, comprised of greenschist to upper-amphibolite facies chlorite and epidote bearing calc-silicate schist, amphibolite, and graphite bearing pelitic schist, rocks that are unconformably overlain by a cover of mostly unmetamorphosed limestone and volcanic rock (Standley and Harris, 2009). Within the metamorphic basement the protoliths of the amphibolites are interpreted to be middle Jurassic (c. 175 Ma) mid-ocean ridge basalt, or arc-related basalts, basaltic-andesites and andesites (Standley and Harris, 2009; Park et al., 2014). These rocks pre-date the intercalated metasedimentary rocks that, on the basis of detrital zircon age data, are interpreted to represent late Cretaceous (<80 Ma) impure limestone and arc derived terrigenous sediment (Standley and Harris, 2009). Both the igneous and sedimentary protoliths of the Banda Terrane were metamorphosed at approximately 45 Ma (Standley and Harris, 2009).

The Aileu Complex (Fig. 1) can be divided into northern and southern sectors. The southern sector is composed mostly of mudstone and shale that, in the southern extreme of this complex, interfinger with the Maubisse Formation (Carter et al., 1976; Barber et al., 1977). The Maubisse Formation is defined by thickly bedded limestone, pink to red calcareous shale, pillow basalt, and felsic volcanoclastic rock (Charlton et al., 2002). On the basis of their fossil assemblages, the limestones of the Maubisse Formation are dated to the latest Carboniferous or early Permian and have strong faunal affinities with age equivalent rocks exposed to the south in Western Australia (Davydov et al., 2013; Haig et al., 2014). Elsewhere, detrital zircon ages and uncommon fossil occurrences suggest the mudstones of the Aileu Complex mostly date to the late Permian or Triassic, although it has also been argued that the sequence could extend into the Jurassic (Brunnschweiler, 1978; Barber et al., 1977; Ely et al., 2014). The southern Aileu Complex thus shows strong lithological and temporal affinities with much of the Gondwana Sequence.

In contrast, the northern sector of the Aileu Complex preserves evidence for multiple phases of folding and records peak metamorphic temperatures of approximately 650 °C (Berry and Grady, 1981). In addition, the easternmost exposures of the complex are dominated by mafic to ultramafic igneous rocks (Berry, 1981; Berry and Jenner, 1982). Thus both the rock types and the degree of deformation and metamorphism observed in the north and east of the Aileu Complex resemble those observed in the Banda Terrane (Barber and Audley-Charles, 1976; Kaneko et al., 2007; Audley-Charles, 2011). As a consequence, Grunau (1953) grouped the rocks of the Aileu Complex with those Banda Terrane. More recent isotopic data has largely precluded this correlation (Standley and Harris, 2009), although the geological differences between the Aileu Complex and the Gondwana Sequence have nevertheless been used to argue that these two sequences are not correlative. Instead a number of studies imply that the Aileu Complex is allochthonous with respect to the Indo-Australian plate.

In addition to the lithologic and metamorphic similarities with the Banda Terrane, this hypothesis is supported by a number of independent lines of evidence. Carter et al. (1976) and Barber et al. (1977) for example noted that the Aileu Complex both fined to the south and, at the faulted contact with the Gondwana Sequence, was juxtaposed against rocks derived from very different depositional environments. North of the Laclo Fault the shallow-water limestones of the Maubisse Formation (Aileu Complex) are exposed, while lying south of this structure are the deep-water shale and mudstone of the Cribas and Atahoc formations (Gondwana Sequence). On the basis of these observations they argued for a northern Sundaland provenance for the Aileu Complex and a southern Indo-Australian origin for the Gondwana Sequence.

A similar conclusion has been drawn based on the timing of deformation and metamorphism in the Aileu Complex. These rocks yield $^{40}Ar/^{39}Ar$ hornblende and biotite cooling ages mostly between 10 and 6 Ma (Berry and McDougall, 1986; Ely et al., 2014), ages that precede by 3–7 million years the inferred timing of arc-continent collision. Collision is thought to have occurred at approximately 3 Ma based on the termination of arc magmatism on Alor, Wetar and Ataúro, the volcanic islands located to the immediate north of Timor (Abbott and Chamalaun, 1981; Audley-Charles, 2011; Ely et al., 2011). The termination of arc magmatism also shortly post-dated the onset of rapid uplift and exhumation of Timor, events constrained by changes in the foraminiferal assemblages preserved in syn-orogenic sediments, and by the widespread cooling of pre-collisional strata through the closure of the zircon and apatite (U-Th)/He isotopic systems (Haig and McCartain, 2007; Haig, 2012; Tate et al., 2014).

Recent dating of metamorphic monazite from the Aileu Complex (5.5–4.7 Ma) suggests a somewhat shorter interval between metamorphism and the onset of collision (Berry et al., 2016). Nevertheless, the variance in the timing of metamorphism and collision has been used to argue that the metamorphic history of the Aileu Complex was not associated with collision in Timor, but rather could owe its origins to the initiation of the Banda Arc (Ely et al., 2014). If correct, the implication is that the Aileu Complex was tectonically emplaced into its present position and, thus, was not an integral component of the pre-collision Indo-Australian plate.

3. Previous geochronological results

The earliest detrital zircon dataset with relevance to the present study is that of Harris (2006). These data were not collected from Timor but from schists interpreted to be correlative with those of the Aileu Complex exposed on the island of Kisar (Fig. 1). The dataset was small, 16 analyses in total, and yielded ages between 300 and 1900 Ma, with the majority close to 300 Ma. Ely et al. (2014) and Spencer et al. (2016) present more extensive datasets for the Aileu Complex and their data reveal major age modes at 270–430 Ma, 860–1180 Ma (Ely et al., 2014 only) and 1460–1870 Ma. Consistent with the findings of Harris (2006), the datasets presented by these studies show that the youngest age population is modally most abundant. Ely et al. (2014) further described the Palaeozoic zircons as mostly euhedral and sub-euhedral in shape, implying a relatively proximal source. This study also described the zircon internal structure and chemistry as being consistent with derivation from a predominantly igneous source.

Kwon et al. (2014) and Zimmermann and Hall (2016) both present U-Pb detrital zircon age data from the Niof and Babulu formations from the Gondwana Sequence. Their datasets are similar and yield major age modes between 200–600 Ma, 800–1200 Ma and 1500–2000 Ma. Petrographic and heavy mineral analysis undertaken by Zimmermann and Hall (2016) indicate that most of the Gondwana Sequence sandstones are comprised of approximately 50% feldspar and lithic fragments, with a heavy mineral assemblage dominated by apatite, zircon, garnet, tourmaline, pyroxene and aluminosilicate. Zircon morphologies were described as a mix of both idiomorphic and rounded grains and interpreted as implying both recycled orogen and magmatic arc type provenance signatures.

Detrital zircon ages similar to those reported by Ely et al. (2014), Kwon et al. (2014), Spencer et al. (2016) and Zimmermann and Hall (2016) were also obtained from modern river sands which sampled in variable proportions all of the major tectonic units in Timor (Dinis et al., 2013). The regional similarity in detrital zircon ages lead Dinis et al. (2013) to the conclusion that the Aileu Complex and the Gondwana Sequence shared a common provenance, although the study also noted that the Aileu Complex was characterised by a lower proportion of Triassic aged zircon when compared to the Gondwana Sequence.

4. Samples and methods

Two sandstone samples from the Gondwana Sequence were selected for U-Pb zircon isotopic analysis (Fig. 2). The first of these samples was collected from the Laclo River valley along the Manatutu–Laclo road (sample LSP-079). The second sample location was an outcrop located approximately 4 km south of Maubisse along the Maubisse-Same road (sample LSP-111). Neither locality has direct stratigraphic age control, although nearby fossil locations reported by Haig and McCartain (2012) suggest both samples were likely collected from the Triassic Babulu Formation.

Sample LSP-079 is a medium-grained yellow-brown sandstone that occurs as decimetre and metre wide layers in a sequence otherwise dominated by finely laminated, similarly coloured mudstone (Fig. 3). Sample LSP111 was collected from an outcrop consisting of intercalated mudstone, marl and sandstone. The sample was collected from a decimetre to metre thick, medium-grained, horizon or purple coloured sandstone. The sampled sandstone layer is interbedded with finely laminated grey-green mudstone.

In addition, twenty-nine samples of fine-grained argillite (mudstone protoliths) were collected from both the Aileu Complex and the Gondwana Sequence for chemical and Nd isotopic analysis (Fig. 2). Sixteen of these samples were collected from well-distributed localities across the eastern half of the Aileu Complex (Fig. 2). The samples from the centre and south of this complex are mudstones and slates, while those from the north and east are phyllites and schists. Samples collected along the north coast overlap with the area from which Ely et al. (2014) report Permo-Triassic maximum depositional ages, while those in the south are proximal to the Maubisse Formation, rocks that have a late Carboniferous or early Permian depositional age (Davydov et al., 2013; Haig et al., 2014). The remaining thirteen samples are from the Gondwana Sequence and were collected mostly within 30 km of the Laclo Fault. The distribution of these samples bound the Aileu Complex to the south and east (Fig. 2) and were probably collected from the Babulu Formation (Haig and McCartain, 2012). It is possible however that some samples are from the Atahoc or Cribas formations, although these units have not yet been positively identified in the study area.

U-Pb zircon ages were measured by Laser Ablation Inductively Coupled Plasma Mass Spectroscopy (LA-ICP-MS). Following the analytical procedure of Paton et al. (2010), a 193 nm excimer laser was used to ablate c. 20 μm diameter pits from single zircon grains. Analysis was undertaken for 50 s, or until the laser penetrated through the zircon into the mounting medium. Zircon standard 91500, with established $^{206}Pb/^{207}Pb$ and $^{206}Pb/^{238}U$ ages of 1065 Ma and 1062 Ma (Wiedenbeck et al., 2004) was used as the primary reference material. The Temora 2 (416.8 ± 1.3 Ma: Black et al., 2004) and Plesovice (337.13 ± 0.37 Ma: Sláma et al., 2008) zircons were used as secondary standards. Zircon 91500 was analysed once every 10–15 unknowns, while analyses of the secondary reference materials were interspersed with those of the unknowns to provide a further calibration check. Eleven analyses of Temora 2 yielded an age of 415.0 ± 0.9 Ma while 12 analyses of the Plesovice zircon yielded an age of 338.4 ± 0.5 Ma.

Reported ages are based on radiogenic $^{207}Pb/^{206}Pb$ for ages >800 Ma and $^{206}Pb/^{238}U$ for ages <800 Ma. The degree of discordance for measured $^{207}Pb/^{206}Pb$ and $^{206}Pb/^{238}U$ ages is given by: $^{207/206}$discordance = [1 − ($^{206}Pb/^{238}U$ age)/($^{207}Pb/^{206}Pb$ age)] × 100 and $^{206/238}$discordance = [1 − ($^{206}Pb/^{238}U$ age)/($^{207}Pb/^{235}U$ age)] × 100. For plotting and data analysis purposes, data are considered concordant when $^{207/206}$discordance ⩽ 10% and $^{206/238}$discordance ⩽ 5%. The U-Pb data are presented in Tables 1 and 2.

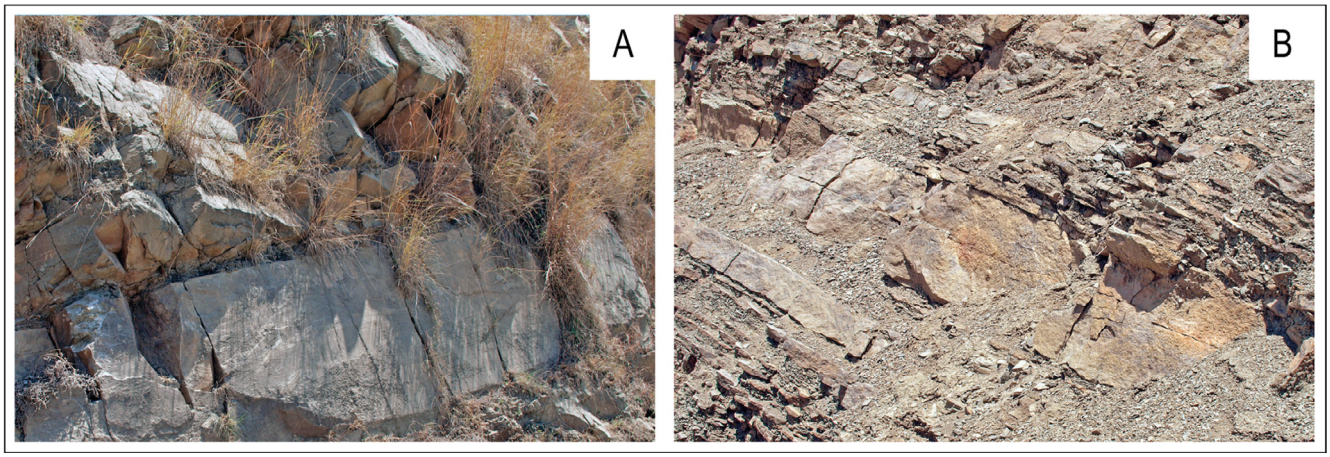

Fig. 3. Outcrop photographs of location LSP-079. (A) Sample location site for LSP-079. Broken edge in the lower left of the photograph is the sample site. (B) Typical outcrop appearance of the Babulu Formation in this region. Note the intercalation of thicker and internally massive sandstone layers with thinner, laminated and more friable mudstone. Sandstone layers in both photographs are approximately 0.5 m thick.

Table 1
U–Pb compositional data for sample LSP–079 (8.5502°S, 125.9343°E). Data in italic text is that used for plotting and analysis.

				Radiogenic ratios							Age (Ma)						
Grain spot	U (ppm)	Th (ppm)	Th/U	$^{207}Pb/^{235}U$	±	$^{206}Pb/^{238}U$	±	$^{207}Pb/^{206}Pb$	±	ρ	$^{207}Pb/^{235}U$	±	$^{206}Pb/^{238}U$	±	$^{207}Pb/^{206}Pb$	±	% Disc
102	194	150	0.77	0.257	0.009	0.036	0.0004	0.050	0.0018	0.33	234	7	*230*	*3*	230	67	1
50	163	92	0.56	0.247	0.015	0.037	0.0011	0.054	0.0036	0.23	225	12	*232*	*7*	350	130	−3
70	766	451	0.59	0.281	0.008	0.038	0.0003	0.054	0.0017	0.29	251	7	*239*	*2*	342	66	5
71	489	567	1.16	0.282	0.005	0.038	0.0003	0.054	0.0011	0.22	253	4	*240*	*2*	354	42	5
36	140	163	1.16	0.274	0.010	0.038	0.0004	0.052	0.0018	0.20	245	8	*241*	*2*	263	67	1
86	264	180	0.68	0.274	0.008	0.038	0.0003	0.052	0.0014	0.15	246	6	*242*	*2*	275	54	2
35	511	538	1.05	0.282	0.009	0.039	0.0005	0.053	0.0018	0.32	252	7	*247*	*3*	304	72	2
98	328	228	0.69	0.289	0.006	0.039	0.0003	0.053	0.0011	0.20	258	5	*248*	*2*	318	43	4
3	258	149	0.57	0.298	0.006	0.040	0.0003	0.055	0.0012	0.35	264	5	*250*	*2*	379	44	5
42	201	136	0.68	0.292	0.007	0.040	0.0003	0.054	0.0013	0.25	260	5	*252*	*2*	360	49	3
1	134	85	0.63	0.286	0.008	0.040	0.0003	0.052	0.0015	0.32	255	6	*255*	*2*	277	55	0
43	303	281	0.93	0.295	0.006	0.040	0.0003	0.053	0.0011	0.25	261	5	*256*	*2*	305	41	2
61	195	136	0.70	0.290	0.007	0.041	0.0003	0.051	0.0014	0.26	259	6	*259*	*2*	238	51	0
51	445	319	0.72	0.314	0.006	0.042	0.0003	0.054	0.0012	0.30	277	5	*266*	*2*	361	46	4
78	112	54	0.48	0.307	0.010	0.042	0.0004	0.054	0.0018	0.23	270	8	*267*	*3*	289	64	1
41	453	654	1.44	0.312	0.005	0.042	0.0003	0.054	0.0008	0.26	276	4	*267*	*2*	341	33	3
74	100	95	0.95	0.294	0.010	0.042	0.0004	0.051	0.0018	0.32	261	8	*268*	*3*	246	66	−2
65	512	129	0.25	0.315	0.006	0.043	0.0004	0.054	0.0010	0.36	278	4	*269*	*3*	338	41	3
97	267	161	0.60	0.305	0.006	0.043	0.0003	0.051	0.0010	0.28	269	5	*274*	*2*	227	42	−2
55	844	712	0.84	0.330	0.006	0.045	0.0003	0.055	0.0011	0.35	290	5	*281*	*2*	380	43	3
12	528	376	0.71	0.326	0.004	0.045	0.0002	0.053	0.0007	0.19	287	3	*284*	*1*	302	28	1
93	212	192	0.91	0.333	0.007	0.047	0.0003	0.052	0.0011	0.28	291	5	*294*	*2*	263	44	−1
9	432	201	0.46	0.360	0.008	0.048	0.0003	0.055	0.0013	0.13	311	6	*303*	*2*	387	50	3
23	313	290	0.93	0.373	0.007	0.050	0.0003	0.055	0.0010	0.27	322	5	*315*	*2*	386	38	2
89	86	98	1.14	0.371	0.016	0.051	0.0006	0.053	0.0024	0.16	323	12	*320*	*4*	348	84	1
47	638	523	0.82	0.393	0.005	0.052	0.0003	0.055	0.0006	0.19	336	4	*327*	*2*	383	26	3
29	1017	1108	1.09	0.391	0.005	0.053	0.0003	0.054	0.0007	0.12	335	4	*332*	*2*	367	29	1
58	518	267	0.52	0.408	0.006	0.053	0.0003	0.056	0.0009	0.26	347	5	*334*	*2*	438	36	4
37	441	250	0.57	0.410	0.012	0.054	0.0006	0.056	0.0018	0.41	349	9	*341*	*3*	451	69	2
24	208	112	0.54	0.400	0.008	0.055	0.0003	0.053	0.0010	0.24	341	6	*347*	*2*	301	40	−2
27	331	286	0.86	0.421	0.008	0.057	0.0004	0.054	0.0010	0.14	356	6	*356*	*2*	360	39	0
100	214	246	1.15	0.475	0.012	0.060	0.0007	0.058	0.0015	0.24	395	8	*376*	*5*	523	53	5
64	347	183	0.53	0.586	0.011	0.072	0.0006	0.060	0.0012	0.32	467	7	*448*	*4*	572	44	4
85	609	443	0.73	0.569	0.010	0.073	0.0006	0.057	0.0010	0.20	457	7	*451*	*3*	494	39	1
90	658	384	0.58	0.585	0.008	0.074	0.0005	0.057	0.0008	0.27	469	5	*460*	*3*	500	31	2
39	130	89	0.68	0.619	0.012	0.075	0.0005	0.060	0.0012	0.36	487	7	*465*	*3*	568	43	5
33	392	55	0.14	0.587	0.008	0.075	0.0004	0.057	0.0008	0.26	469	5	*468*	*2*	472	30	0
21	541	643	1.19	0.650	0.007	0.082	0.0004	0.057	0.0007	0.35	508	4	*506*	*2*	501	25	0
5	557	592	1.06	0.799	0.008	0.094	0.0005	0.062	0.0007	0.24	597	5	*579*	*3*	678	23	3
62	781	198	0.25	1.093	0.007	0.121	0.0005	0.065	0.0004	0.19	749	4	*738*	*3*	786	13	1
30	211	133	0.63	1.078	0.015	0.122	0.0007	0.065	0.0009	0.27	742	7	*745*	*4*	748	30	0
48	346	561	1.62	1.311	0.014	0.141	0.0007	0.068	0.0007	0.22	850	6	848	4	*852*	*22*	0
53	377	306	0.81	1.354	0.024	0.142	0.0015	0.070	0.0011	0.05	871	11	856	8	*944*	*31*	9
73	567	157	0.28	1.618	0.011	0.162	0.0006	0.073	0.0005	0.22	976	4	968	3	*1004*	*13*	4
32	297	270	0.91	1.699	0.020	0.167	0.0010	0.075	0.0009	0.24	1008	7	995	5	*1063*	*23*	6
45	978	1094	1.12	1.687	0.015	0.164	0.0008	0.076	0.0006	0.28	1004	6	981	5	*1082*	*15*	9
16	174	125	0.72	2.143	0.021	0.198	0.0008	0.079	0.0008	0.29	1163	7	1163	5	*1174*	*20*	1
69	538	453	0.84	2.039	0.023	0.185	0.0014	0.079	0.0008	0.23	1129	8	1096	8	*1184*	*20*	7
59	482	32	0.07	3.283	0.019	0.248	0.0010	0.096	0.0005	0.15	1477	5	1427	5	*1539*	*9*	7
94	496	101	0.20	3.549	0.019	0.267	0.0009	0.096	0.0005	0.21	1538	4	1526	5	*1547*	*9*	1
60	517	87	0.17	3.685	0.027	0.278	0.0014	0.096	0.0007	0.35	1568	6	1582	7	*1548*	*13*	−2
99	245	112	0.46	3.539	0.025	0.266	0.0011	0.096	0.0007	0.31	1535	6	1519	6	*1553*	*13*	2
67	619	133	0.21	3.375	0.023	0.252	0.0012	0.097	0.0007	0.34	1499	5	1450	6	*1562*	*13*	7
2	417	181	0.43	3.890	0.019	0.288	0.0010	0.098	0.0004	0.22	1612	4	1630	5	*1590*	*8*	−2
92	295	65	0.22	3.933	0.032	0.290	0.0017	0.099	0.0008	0.30	1619	7	1643	9	*1602*	*14*	−3
66	264	224	0.85	3.809	0.027	0.279	0.0013	0.099	0.0006	0.26	1595	6	1586	7	*1602*	*12*	1
10	209	145	0.69	3.459	0.031	0.253	0.0017	0.100	0.0008	0.23	1519	7	1451	9	*1620*	*15*	10
91	235	125	0.53	4.400	0.040	0.298	0.0020	0.107	0.0010	0.26	1714	8	1685	10	*1754*	*16*	4
31	299	220	0.74	4.525	0.030	0.305	0.0014	0.108	0.0007	0.32	1735	6	1716	7	*1770*	*11*	3
13	233	68	0.29	4.608	0.033	0.308	0.0013	0.109	0.0008	0.37	1750	6	1731	7	*1786*	*13*	3
11	370	174	0.47	5.337	0.048	0.333	0.0022	0.116	0.0008	0.18	1874	8	1851	11	*1902*	*13*	3
15	49	29	0.60	10.670	0.091	0.466	0.0024	0.166	0.0015	0.22	2495	8	2468	11	*2518*	*15*	2
54	1064	411	0.39	0.281	0.006	0.032	0.0003	0.065	0.0013	0.24	252	5	201	2	779	43	20
96	694	343	0.49	0.267	0.004	0.034	0.0002	0.056	0.0008	0.21	240	3	*217*	*1*	448	31	9
25	559	950	1.70	0.266	0.004	0.035	0.0003	0.056	0.0009	0.25	239	3	*219*	*2*	452	33	8
19	35	25	0.74	0.297	0.021	0.036	0.0007	0.062	0.0046	0.37	254	17	*226*	*5*	370	140	11
44	60	50	0.83	0.236	0.013	0.037	0.0005	0.047	0.0026	0.23	211	11	*233*	*3*	44	92	−10
6	1098	1018	0.93	0.287	0.006	0.037	0.0003	0.057	0.0011	0.15	256	5	*235*	*2*	458	44	8
72	299	153	0.51	0.325	0.014	0.038	0.0005	0.062	0.0027	0.31	284	10	*242*	*3*	626	87	15
17	156	152	0.97	0.344	0.010	0.042	0.0004	0.059	0.0018	0.24	299	8	*265*	*3*	511	62	11
38	148	95	0.64	0.371	0.009	0.043	0.0004	0.064	0.0016	0.17	322	7	271	2	691	51	16
68	190	128	0.67	0.355	0.012	0.044	0.0005	0.059	0.0020	0.25	307	9	*277*	*3*	517	72	10

(*continued on next page*)

Table 1 (*continued*)

Grain spot	U (ppm)	Th (ppm)	Th/U	Radiogenic ratios							Age (Ma)						
				$^{207}Pb/^{235}U$	±	$^{206}Pb/^{238}U$	±	$^{207}Pb/^{206}Pb$	±	ρ	$^{207}Pb/^{235}U$	±	$^{206}Pb/^{238}U$	±	$^{207}Pb/^{206}Pb$	±	% Disc
18	64	33	0.51	0.300	0.012	0.044	0.0005	0.050	0.0020	0.27	262	9	*278*	*3*	168	73	−6
8	414	367	0.89	0.486	0.008	0.060	0.0004	0.059	0.0009	0.12	402	5	*375*	*2*	550	33	7
87	316	312	0.99	0.594	0.010	0.069	0.0005	0.063	0.0010	0.24	474	6	*431*	*3*	687	34	9
14	1305	915	0.70	1.897	0.033	0.139	0.0023	0.100	0.0006	0.17	1078	11	839	13	1620	11	48
83	688	283	0.41	1.723	0.015	0.163	0.0009	0.077	0.0006	0.18	1017	5	973	5	*1126*	*15*	14
82	284	116	0.41	1.942	0.021	0.178	0.0012	0.080	0.0008	0.25	1095	7	1056	6	*1186*	*20*	11
79	143	72	0.50	2.334	0.032	0.196	0.0013	0.087	0.0011	0.17	1224	10	1155	7	*1359*	*25*	15
75	271	216	0.80	3.903	0.062	0.265	0.0028	0.109	0.0017	0.23	1613	13	1517	14	*1772*	*28*	14

Table 2
U–Pb compositional data for sample LSP–111 (8.8579°S, 125.5843°E). Data in italic text is that used for plotting and analysis.

Grain spot	U (ppm)	Th (ppm)	Th/U	Radiogenic ratios							Age (Ma)						
				$^{207}Pb/^{235}U$	±	$^{206}Pb/^{238}U$	±	$^{207}Pb/^{206}Pb$	±	ρ	$^{207}Pb/^{235}U$	±	$^{206}Pb/^{238}U$	±	$^{207}Pb/^{206}Pb$	±	% Disc
46	266	211	0.79	0.287	0.013	0.041	0.0006	0.050	0.0024	0.255	254	10	*260*	*4*	205	85	−2
51	579	404	0.70	0.315	0.013	0.042	0.0005	0.055	0.0023	0.107	277	10	*264*	*3*	360	84	5
15	333	468	1.40	0.490	0.019	0.064	0.0009	0.056	0.0022	0.215	405	13	*398*	*5*	414	79	2
64	176	100	0.57	0.511	0.021	0.067	0.0008	0.056	0.0023	0.229	412	14	*417*	*5*	349	79	−1
6	1050	125	0.12	0.575	0.013	0.071	0.0008	0.059	0.0014	0.344	461	9	*440*	*5*	537	54	5
45	435	203	0.47	0.689	0.021	0.085	0.0009	0.060	0.0019	0.246	532	13	*524*	*5*	556	68	2
41	17	92	5.42	0.972	0.096	0.091	0.0030	0.081	0.0086	0.247	583	54	*564*	*18*	540	200	3
20	116	87	0.75	0.736	0.039	0.092	0.0018	0.058	0.0032	0.271	557	22	*567*	*10*	460	110	−2
3	1147	1566	1.37	0.776	0.012	0.092	0.0006	0.061	0.0009	0.279	582	7	*570*	*4*	619	34	2
31	271	78	0.29	0.814	0.022	0.095	0.0011	0.061	0.0017	0.285	602	12	*584*	*6*	602	59	3
13	140	83	0.59	0.801	0.032	0.099	0.0014	0.058	0.0023	0.244	597	18	*607*	*9*	494	80	−2
33	43	1	0.03	0.880	0.063	0.099	0.0026	0.064	0.0047	0.047	596	35	*610*	*15*	410	130	−2
34	106	78	0.74	0.942	0.039	0.113	0.0017	0.060	0.0025	0.233	668	20	*688*	*10*	549	83	−3
23	170	169	1.00	1.550	0.052	0.155	0.0020	0.074	0.0024	0.188	952	21	927	11	*1000*	*68*	7
12	467	201	0.43	1.792	0.029	0.171	0.0016	0.076	0.0012	0.226	1039	11	1015	9	*1091*	*32*	7
9	95	96	1.01	2.174	0.064	0.199	0.0026	0.079	0.0024	0.238	1166	21	1168	14	*1164*	*62*	0
61	108	66	0.62	2.195	0.046	0.198	0.0020	0.080	0.0017	0.276	1180	15	1160	11	*1187*	*43*	2
55	286	120	0.42	2.141	0.041	0.195	0.0018	0.080	0.0016	0.265	1158	13	1147	10	*1188*	*39*	3
30	62	1	0.02	2.269	0.086	0.201	0.0034	0.082	0.0033	0.311	1195	27	1180	18	*1197*	*81*	1
66	238	22	0.09	2.390	0.048	0.210	0.0021	0.082	0.0017	0.323	1238	14	1230	11	*1233*	*42*	0
5	378	79	0.21	2.566	0.036	0.217	0.0016	0.086	0.0013	0.288	1289	10	1265	9	*1330*	*28*	5
21	235	140	0.59	3.358	0.076	0.261	0.0028	0.093	0.0021	0.251	1494	18	1494	15	*1485*	*42*	−1
14	169	200	1.18	3.493	0.069	0.261	0.0025	0.097	0.0018	0.211	1522	16	1493	13	*1558*	*36*	4
16	237	296	1.25	4.076	0.075	0.286	0.0040	0.103	0.0020	0.395	1648	15	1623	20	*1673*	*35*	3
47	270	160	0.59	4.136	0.097	0.280	0.0034	0.109	0.0025	0.272	1662	19	1593	17	*1773*	*43*	10
10	494	42	0.09	4.548	0.042	0.303	0.0021	0.109	0.0010	0.331	1739	8	1705	11	*1776*	*16*	4
25	187	45	0.24	4.928	0.081	0.313	0.0033	0.113	0.0018	0.276	1811	14	1757	16	*1856*	*31*	5
32	241	280	1.16	4.995	0.067	0.309	0.0028	0.116	0.0014	0.255	1818	11	1738	14	*1889*	*22*	8
18	581	271	0.47	5.750	0.110	0.331	0.0052	0.126	0.0022	0.303	1940	17	1840	25	*2041*	*31*	10
63	580	322	0.56	7.630	0.089	0.387	0.0030	0.143	0.0016	0.326	2188	10	2111	14	*2260*	*19*	7
1	395	441	1.12	13.400	0.110	0.512	0.0035	0.189	0.0014	0.385	2709	8	2667	15	*2733*	*13*	2
52	191	58	0.30	19.890	0.230	0.594	0.0063	0.243	0.0023	0.258	3087	12	3006	25	*3138*	*15*	4
54	118	80	0.68	0.251	0.016	0.031	0.0006	0.062	0.0042	0.294	220	13	194	4	400	120	12
29	481	465	0.97	0.272	0.013	0.033	0.0005	0.064	0.0034	0.385	235	9	207	3	507	83	12
36	224	210	0.94	0.313	0.015	0.034	0.0006	0.066	0.0033	0.27	279	11	218	3	700	97	22
27	92	93	1.01	0.384	0.042	0.040	0.0013	0.068	0.0080	0.271	307	31	255	8	520	220	17
69	904	793	0.88	0.358	0.013	0.046	0.0007	0.057	0.0021	0.266	311	10	289	5	452	78	7
37	134	76	0.57	0.327	0.020	0.048	0.0008	0.050	0.0032	0.231	277	16	300	5	110	110	−8
53	168	250	1.49	0.403	0.026	0.051	0.0010	0.056	0.0037	0.231	348	18	323	6	430	120	7
39	96	66	0.69	0.391	0.022	0.060	0.0009	0.049	0.0028	0.208	325	17	373	6	74	95	−15
19	795	84	0.11	1.507	0.038	0.146	0.0020	0.075	0.0020	0.322	930	16	877	11	1069	53	18
42	22	15	0.69	1.680	0.210	0.161	0.0075	0.081	0.0100	0.062	970	87	959	41	820	250	−17
40	329	270	0.82	1.817	0.050	0.168	0.0024	0.078	0.0020	0.154	1051	18	1001	14	1150	50	13
62	520	189	0.36	1.867	0.053	0.171	0.0025	0.079	0.0025	0.366	1072	19	1015	14	1163	63	13
26	460	383	0.83	2.042	0.047	0.178	0.0024	0.083	0.0019	0.335	1129	16	1054	13	1275	45	17
35	187	509	2.72	2.132	0.053	0.185	0.0025	0.084	0.0022	0.342	1158	17	1097	14	1286	51	15
4	142	198	1.39	2.265	0.050	0.195	0.0018	0.084	0.0019	0.248	1200	15	1146	10	1283	44	11
28	242	192	0.79	3.731	0.098	0.261	0.0042	0.104	0.0025	0.146	1579	21	1495	21	1700	44	12
50	336	98	0.29	4.134	0.063	0.276	0.0024	0.109	0.0016	0.241	1661	12	1573	12	1773	27	11

Major element abundances were determined by inductively coupled plasma-atomic emission spectroscopy (ICP-AES), using solutions made from approximately 5 g of dissolved sample material. For trace element and Sm-Nd isotopic work, approximately 70 mg of sample material was dissolved at high pressure. Trace element concentrations (including REE) were

determined by ICP-MS (Agilent 7700×) on a ~10% split of the clear (except for some undissolved graphite flakes) solutions, using methods adapted from Eggins et al. (1997) with the USGS basalt W-2 used as primary calibration standard. Nd was extracted from the remaining solution using small columns of EICHROM TRUspec and LNspec resin (Pin and Zalduegui, 1997; Maas et al., 2015). Nd isotope ratios were measured on a NU Plasma multi-collector ICP-MS with sample uptake via a CETAC Aridus desolvation system (Woodhead, 2002). Data were acquired on solutions containing 100–120 ppb Nd (15–20 V total Nd signal). Instrumental mass bias was corrected by internal normalisation to $^{146}Nd/^{144}Nd = 0.7219$ using the exponential law, and data are reported relative to a $^{143}Nd/^{144}Nd$ of 0.511860 for the La Jolla Nd standard, which was measured after each three unknowns in every session. The JNd-1 Nd isotope standard averages 0.512114 ± 16 (2sd) while the BCR-2 basalt standard yields a long-term average of 0.512641 ± 24 (2sd), consistent with published reference values. These results indicate an external precision of ±0.000020 (2sd). Age corrections for $^{143}Nd/^{144}Nd$ are based on $^{147}Sm/^{144}Nd$ ratios calculated from the trace element data for the same sample solutions. For a subset of solutions, Sm/Nd ratios were also determined by isotope dilution with a ^{149}Sm-^{150}Nd spike, with excellent agreement of Sm/Nd ratios (within 1.5%) and Sm-Nd concentrations (within 4%) between the two methods. The chemical data and Sm-Nd isotopic data are presented in Tables 3–6 and 7, respectively.

5. Results

5.1. U-Pb geochronology

Zircons from sample LSP-079 are mostly colourless to yellow and vary morphologically from euhedral to rounded. Aspect ratios are generally <3:1 and grain lengths are between 20 and 250 μm. Most grains show a cathodoluminescent (CL) response characterised by concentric oscillatory zonation. This suggests a probable magmatic origin, an inference consistent with Th/U values generally >0.1 (Table 1). Eighty zircon grains were analysed from this sample and, of these, sixty-two yielded concordant results (Fig. 4). Given the number of concordant results, the probability of missing an age population >10% of the total is approximately 1% (Vermeesch, 2004).

The ages obtained from sample LSP-079 are between 230 Ma and 2000 Ma with a single outlier at 2520 Ma (Table 1). The two youngest grains give a weighted mean $^{206}Pb/^{238}U$ age of 230 ± 3 Ma, which is taken to provide a maximum depositional age for the sampled rock. This is consistent with the late Triassic depositional age inferred for the Balulu Formation (Haig and McCartain, 2012).

The zircon age distribution shows several peaks, the largest of which occurs between 230 and 400 Ma. This population is defined by just over 50% of the concordant data (Fig. 4) and contains two modal maxima. The larger of these yields a mean age of approximately 260 Ma, while the smaller age maxima is at approximately

Table 3
Whole rock data for argillitic sediments from the Aileu Complex. Sample locations given in Fig. 2.

	High Silica (SiO_2 > 63 wt%)													Low Silica (SiO_2 < 63 wt%)			
Sample	LSP013	LSP076	LSP084	LSP099	LSP102	RIL031	RIL047	RIL061	RIL075	RIL077	RIL169	RIL196	TKI066	TKI036	RIL067	RIL228	Mean
SiO_2	67.6	65.6	67.6	67.5	70.9	65.8	69.7	63.7	63.8	64.1	63.9	66.8	64.7	60.1	62.2	58.5	65.1
TiO_2	0.68	0.76	0.64	0.69	0.67	0.71	0.87	0.72	0.69	0.73	0.75	0.71	0.68	0.78	0.75	0.63	0.72
Al_2O_3	16.0	16.1	16.7	16.3	16.0	16.9	14.0	17.5	18.6	17.1	17.9	16.3	17.1	18.9	16.2	15.1	16.7
FeO	4.99	5.92	4.63	3.96	5.54	5.45	4.80	6.14	5.32	6.00	5.20	5.16	4.72	6.34	7.03	6.91	5.51
MnO	0.05	0.06	0.11	0.03	0.06	0.02	0.07	0.03	0.03	0.10	0.01	0.05	0.19	0.15	0.09	0.08	0.07
MgO	1.98	1.96	1.29	1.70	1.81	1.89	1.79	2.18	1.69	1.83	1.76	2.06	2.33	2.06	2.50	2.72	1.97
CaO	0.95	0.15	0.81	0.28	0.41	0.02	0.72	0.01	0.02	0.13	0.41	0.13	1.27	2.09	0.85	1.77	0.63
Na_2O	0.97	1.35	1.54	2.98	1.66	1.05	0.49	0.95	0.94	1.36	0.91	1.48	1.83	2.39	2.19	1.26	1.46
K_2O	4.60	3.67	4.04	3.26	3.57	4.12	2.58	4.06	4.32	4.15	4.39	3.71	3.99	4.06	3.68	3.67	3.87
P_2O_5	0.15	0.08	0.05	0.10	0.07	0.11	0.10	0.10	0.02	0.09	0.14	0.13	0.04	0.14	0.16	0.13	0.10
Total	98.0	95.6	97.4	96.8	100.6	96.1	95.1	95.3	95.5	95.6	95.3	96.6	96.9	97.0	95.7	90.7	
K_2O/Na_2O	4.7	2.7	2.6	1.1	2.2	3.9	5.3	4.3	4.6	3.1	4.8	2.5	2.2	1.7	1.7	2.9	3.1
Mg#	0.28	0.25	0.22	0.30	0.25	0.26	0.27	0.26	0.24	0.23	0.25	0.29	0.33	0.25	0.26	0.28	0.26

Table 4
Whole rock data for argillitic sediments from the Gondwana Sequence. Sample locations given in Fig. 2. HS = High Silica (SiO_2 > 63wt%).

	HS	Low Silica (SiO_2 < 63 wt%)											
Sample	OLI052	LSP077	LSP078	LSP111	LSP118	LSP122	LSP141	OLI040	OLI041	RIL024	RIL029	RIL181	Mean
SiO_2	65.4	57.8	62.9	49.9	62.7	60.4	62.0	56.4	61.1	57.1	61.6	60.9	59.8
TiO_2	0.84	0.75	0.70	0.70	0.87	0.83	0.87	0.34	0.86	0.93	0.78	0.64	0.76
Al_2O_3	16.9	17.3	18.1	16.5	18.5	19.1	18.7	9.4	19.0	21.6	16.3	13.9	17.1
FeO	5.71	6.62	6.66	7.61	7.50	8.01	6.19	4.58	6.75	7.56	5.05	11.52	6.98
MnO	0.02	0.10	0.02	0.13	0.11	0.02	0.05	0.04	0.11	0.04	0.05	0.13	0.07
MgO	1.25	2.05	1.84	2.46	1.24	1.40	1.89	1.33	1.82	1.81	1.91	3.22	1.85
CaO	0.51	3.60	0.79	7.77	0.48	0.82	0.28	12.27	0.32	0.67	3.31	1.33	2.68
Na_2O	1.74	1.88	1.13	1.99	1.60	1.37	1.79	0.75	1.78	1.34	1.84	1.36	1.55
K_2O	2.91	2.62	3.42	3.60	2.38	2.43	2.50	1.68	2.57	3.77	2.73	1.35	2.66
P_2O_5	0.07	0.07	0.05	0.05	0.10	0.12	0.12	0.07	0.12	0.08	0.11	0.05	0.08
Total	95.3	92.7	95.6	90.7	95.4	94.5	94.3	86.8	94.4	94.9	93.7	94.4	
K_2O/Na_2O	1.7	1.4	3.0	1.8	1.5	1.8	1.4	2.2	1.4	2.8	1.5	1.0	1.8
Mg#	0.18	0.24	0.22	0.24	0.14	0.15	0.23	0.23	0.21	0.19	0.27	0.22	0.21

Table 5
Trace and rare earth element data for argillitic sediments from the Aileu Complex.

	High Silica (SiO_2 > 63 wt%)													Low Silica (SiO_2 < 63 wt%)			
Sample	LSP013	LSP076	LSP084	LSP099	LSP102	RIL031	RIL047	RIL061	RIL075	RIL077	RIL169	RIL196	TKI066	TKI036	RIL067	RIL228	Mean
Sc	12	14	11	12	13	15	14	21	15	16	15	14	13	15	16	13	14
Ti	3699	4321	3667	4075	4762	4091	4989	5177	4020	4251	4313	4132	4966	5662	4447	3690	4391
V	84	123	111	79	100	96	126	125	112	97	96	102	142	126	111	89	107
Cr	56	83	46	55	59	65	52	80	72	66	67	67	68	75	84	58	66
Ni	19	29	17	10	–	26	26	33	45	26	25	23	–	–	35	27	26
Ga	19	20	23	19	21	22	19	28	25	23	23	21	24	25	22	20	22
Rb	192	165	194	147	174	198	94	302	217	218	205	174	146	192	184	181	186
Sr	79	41	70	110	75	30	23	32	38	46	40	34	116	117	69	108	64
Y	26	31	51	41	31	34	37	50	29	37	35	33	55	38	34	28	37
Zr	169	223	139	189	211	196	168	233	192	201	208	215	217	273	190	165	199
Nb	16	17	24	16	21	16	29	20	21	18	18	17	37	25	18	16	21
Cs	8.7	6.6	9.4	5.8	8.1	7.6	4.8	12.9	10.6	10.6	9.3	7.5	5.5	8.5	10.6	10.6	8.6
Ba	534	561	471	446	509	463	315	766	478	636	591	518	660	563	605	456	536
La	37	50	66	34	23	47	52	75	47	60	52	48	50	57	55	41	50
Ce	72	103	123	74	110	97	126	151	103	125	104	99	90	120	115	83	106
Pr	8.1	11.5	15.1	8.8	6.6	11.3	13.2	16.9	11.2	13.6	12.4	11.4	12.4	13.1	12.9	9.6	11.7
Nd	29	41	54	32	24	41	50	61	40	49	45	41	47	47	46	35	43
Sm	5.5	7.9	10.3	6.5	4.8	8.1	10.2	11.8	7.5	9.1	8.6	7.7	9.8	9.0	8.8	6.7	8.3
Eu	1.12	1.43	2.21	1.17	0.88	1.38	1.74	2.12	1.19	1.59	1.52	1.32	1.76	1.70	1.61	1.17	1.49
Gd	4.83	6.63	9.31	5.64	4.34	6.94	9.03	10.51	6.12	7.74	7.43	6.54	8.67	7.97	7.49	5.86	7.19
Tb	0.76	1.02	1.49	0.97	0.73	1.07	1.33	1.60	0.96	1.19	1.14	1.04	1.32	1.27	1.14	0.91	1.12
Dy	4.65	5.96	8.96	6.42	4.84	6.34	7.30	9.16	5.58	6.99	6.62	6.19	8.42	7.21	6.58	5.36	6.66
Ho	0.98	1.21	1.93	1.48	1.07	1.28	1.40	1.83	1.13	1.41	1.34	1.28	1.80	1.49	1.33	1.09	1.38
Er	2.83	3.35	5.60	4.48	3.41	3.57	3.65	5.00	3.19	3.91	3.72	3.57	5.47	4.28	3.68	3.00	3.92
Tm	0.44	0.50	0.88	0.70	0.58	0.54	0.52	0.75	0.48	0.59	0.56	0.55	0.85	0.66	0.55	0.46	0.60
Yb	2.88	3.24	5.81	4.47	3.38	3.46	3.24	4.72	3.12	3.75	3.58	3.53	5.12	4.31	3.51	2.94	3.82
Lu	0.42	0.47	0.84	0.59	0.52	0.51	0.46	0.69	0.45	0.55	0.52	0.52	0.73	0.59	0.51	0.43	0.55
Hf	4.72	6.36	4.13	5.26	5.80	5.35	4.69	6.47	5.69	5.59	5.72	5.97	5.60	7.70	5.26	4.54	5.55
Ta	1.21	1.28	1.68	1.38	1.60	1.33	1.78	1.69	1.66	1.47	1.45	1.43	2.40	2.10	1.46	1.27	1.57
W	168	2	117	121	201	49	24	56	43	37	9	21	359	149	37	22	88
Th	18	21	24	18	22	19	14	32	23	25	21	18	21	26	23	19	21
U	3.13	2.74	3.81	4.29	3.46	3.46	2.54	4.75	2.85	3.91	3.54	3.15	3.20	4.11	2.69	2.96	3.41
$(La/Lu)_N$	9.3	11.3	8.4	6.1	4.8	10.0	12.1	11.6	11.1	11.7	10.7	9.9	7.5	10.4	11.7	10.1	9.8
$(Gd/Lu)_N$	1.4	1.7	1.4	1.2	1.0	1.7	2.4	1.9	1.7	1.7	1.8	1.6	1.5	1.7	1.8	1.7	1.6
EuN/Eu*	0.7	0.6	0.7	0.6	0.6	0.6	0.6	0.6	0.5	0.6	0.6	0.6	0.6	0.6	0.6	0.6	0.6
Th/Sc	1.4	1.6	2.1	1.5	1.7	1.3	1.0	1.5	1.5	1.6	1.4	1.3	1.6	1.8	1.5	1.4	1.5
Ti/Zr	21.8	19.4	26.4	21.6	22.6	20.9	29.6	22.2	20.9	21.1	20.8	19.2	22.9	20.7	23.4	22.3	22.2
Rb/Sr	2.4	4.0	2.8	1.3	2.3	6.6	4.0	9.4	5.7	4.7	5.1	5.1	1.3	1.6	2.7	1.7	3.8

Table 6
Trace and rare earth element data for argillitic sediments from the Gondwana Sequence. HS = High Silica (SiO_2 > 63 wt%).

	HS	Low Silica (SiO_2 < 63 wt%)											
Sample	OLI052	LSP077	LSP078	LSP111	LSP118	LSP122	LSP141	OLI040	OLI041	RIL024	RIL029	RIL181	Mean
Sc	13.3	13.0	17.9	14.8	18.0	15.9	18.2	11.8	18.0	20.2	16.1	12.9	15.8
Ti	4852	4296	4206	4228	4857	4655	4968	1983	4865	5344	4524	3772	4379.1
V	104	102	108	143	122	126	126	72	127	116	107	76	110.8
Cr	60	54	77	50	79	79	81	56	79	93	79	44	69.3
Ni	22	36	59	67	39	48	38	47	39	42	36	43	43.2
Ga	21	24	25	24	22	22	22	11	22	26	19	19	21.4
Rb	113	111	197	164	128	124	122	98	128	178	120	56	128.3
Sr	84	118	135	126	106	92	142	305	148	115	142	85	133.2
Y	28	27	16	25	25	25	26	20	28	27	26	23	24.6
Zr	303	225	130	176	188	176	190	68	180	171	163	261	185.9
Nb	22.4	20.9	15.0	22.8	12.1	12.1	11.6	7.4	11.8	21.9	13.2	20.0	15.9
Cs	11.1	6.9	13.0	10.2	9.0	6.4	7.0	6.2	8.1	11.7	8.4	4.0	8.5
Ba	365	439	382	432	342	354	192	292	205	365	235	322	327.1
La	42	42	34	49	33	31	34	27	34	46	30	32	36.1
Ce	88	94	62	109	67	61	71	39	71	88	61	75	73.8
Pr	10	10	7	10	8	7	8	6	8	10	7	8	8.3
Nd	36.4	36.3	24.2	36.1	27.4	25.8	31.4	20.8	32.2	35.5	27.6	27.3	30.1
Sm	6.6	6.8	3.4	6.6	5.2	5.0	6.0	3.7	6.6	5.9	5.4	4.9	5.5
Eu	1.09	1.19	0.53	1.29	1.02	0.95	1.15	0.62	1.33	0.98	1.04	0.91	1.0
Gd	5.18	5.06	2.11	5.54	4.01	3.88	4.55	3.29	5.24	4.60	4.88	4.15	4.4
Tb	0.87	0.82	0.39	0.91	0.67	0.65	0.73	0.52	0.82	0.75	0.76	0.72	0.7
Dy	5.46	5.12	2.74	5.23	4.30	4.33	4.66	3.30	5.13	4.81	4.71	4.40	4.5
Ho	1.15	1.07	0.65	1.06	0.96	0.97	1.03	0.71	1.10	1.06	0.99	0.93	1.0
Er	3.22	3.01	2.05	2.93	2.88	2.86	3.03	2.05	3.21	3.14	2.88	2.69	2.8

Table 6 (*continued*)

	HS	Low Silica (SiO_2 < 63 wt%)											
Sample	OLI052	LSP077	LSP078	LSP111	LSP118	LSP122	LSP141	OLI040	OLI041	RIL024	RIL029	RIL181	Mean
Tm	0.50	0.46	0.34	0.45	0.46	0.44	0.48	0.31	0.49	0.50	0.45	0.43	0.4
Yb	3.26	3.01	2.32	2.91	3.10	2.93	3.14	2.06	3.26	3.15	2.81	2.88	2.9
Lu	0.48	0.44	0.35	0.44	0.46	0.44	0.46	0.30	0.48	0.47	0.43	0.44	0.4
Hf	8.47	6.17	3.65	4.90	5.14	4.96	5.29	1.95	5.05	5.00	4.67	6.98	5.2
Ta	1.53	1.45	1.14	1.53	0.94	0.90	0.92	0.51	0.92	1.59	1.04	1.27	1.1
W	2	2	6	11	16	2	2	1	2	12	17	70	11.9
Th	16	16	15	17	14	14	14	7	15	19	13	12	14.4
U	2.7	2.4	2.4	1.5	3.0	2.6	3.0	3.1	3.0	3.0	2.5	1.8	2.6
$(La/Lu)_N$	9.4	10.2	10.5	12.0	7.7	7.6	7.8	9.5	7.5	10.5	7.6	7.8	9.0
$(Gd/Lu)_N$	1.3	1.4	0.7	1.6	1.1	1.1	1.2	1.4	1.3	1.2	1.4	1.2	1.2
EuN/Eu*	0.6	0.6	0.6	0.7	0.7	0.7	0.7	0.5	0.7	0.6	0.6	0.6	0.6
Th/Sc	1.2	1.2	0.8	1.1	0.8	0.9	0.8	0.6	0.8	0.9	0.8	1.0	0.9
Ti/Zr	16.0	19.1	32.4	24.1	25.8	26.5	26.2	29.1	27.0	31.2	27.8	14.5	25.0
Rb/Sr	1.4	0.9	1.5	1.3	1.2	1.3	0.9	0.3	0.9	1.5	0.8	0.7	1.0

Table 7
Nd isotopic data for argillitic sediments from the Aileu Complex and the Gondwana Sequence. Age (Ma) = the inferred depositional age and is used to calculate initial εNd values. Nd model age is single stage and based on the linear mantle evolution curve of Goldstein et al. (1984) and calculated using the parameters: $^{147}Sm/^{144}Nd = 0.1967$ and $^{143}/^{144}Nd = 0.512638$ for modern CHUR, and εNd = +10 for modern depleted mantle (equivalent to $^{143}/^{144}Nd = 0.513151$).

							εNd		Nd model age (Ga)
Sample	Age (Ma)	Tectonic domain	Sm (ppm)	Nd (ppm)	$^{147}Sm/^{144}Nd$	$^{143}Nd/^{144}Nd$	Present	Initial	
LSP077	230	Gondwana Seq.	6.51	35.27	0.1114	0.512112	−10.1	−7.8	1.55
LSP078	230	Gondwana Seq.	3.40	24.16	0.0851	0.512074	−10.9	−7.7	1.28
LSP111	230	Gondwana Seq.	6.58	36.14	0.1102	0.512201	−8.4	−6.0	1.40
LSP118	230	Gondwana Seq.	5.19	27.41	0.1146	0.512228	−7.9	−5.6	1.42
LSP122	230	Gondwana Seq.	4.82	24.96	0.1166	0.512235	−7.7	−5.5	1.44
LSP141	230	Gondwana Seq.	5.77	30.52	0.1141	0.512311	−6.3	−4.0	1.29
OLI040	230	Gondwana Seq.	3.55	20.07	0.1067	0.512128	−9.8	−7.3	1.46
OLI041	230	Gondwana Seq.	6.37	31.37	0.1226	0.512290	−6.7	−4.6	1.44
OLI052	230	Gondwana Seq.	6.39	35.28	0.1093	0.512080	−10.8	−8.3	1.56
RIL024	230	Gondwana Seq.	5.93	35.40	0.1012	0.512034	−11.7	−9.0	1.51
RIL029	230	Gondwana Seq.	5.37	27.25	0.1189	0.512194	−8.5	−6.4	1.54
RIL047	300	Gondwana Seq.	10.23	50.03	0.1240	0.512144	−9.5	−6.9	1.71
RIL181	230	Gondwana Seq.	4.90	27.31	0.1080	0.512057	−11.2	−8.7	1.58
LSP013	250	Aileu Complex	5.52	28.94	0.1154	0.511907	−14.1	−11.7	1.92
LSP076	250	Aileu Complex	7.59	40.05	0.1143	0.511812	−16.0	−13.5	2.05
LSP084	250	Aileu Complex	10.34	53.92	0.1160	0.511996	−12.4	−10.0	1.80
LSP099	250	Aileu Complex	6.52	32.38	0.1218	0.511890	−14.5	−12.2	2.09
LSP102	250	Aileu Complex	4.71	23.23	0.1225	0.511869	−14.9	−12.6	2.14
RIL031	250	Aileu Complex	8.05	41.27	0.1180	0.511981	−12.7	−10.3	1.86
RIL061	250	Aileu Complex	11.82	61.45	0.1160	0.511908	−14.1	−11.7	1.94
RIL067	250	Aileu Complex	8.81	46.46	0.1150	0.511804	−16.2	−13.7	2.07
RIL075	250	Aileu Complex	7.51	40.19	0.1130	0.511956	−13.2	−10.6	1.81
RIL077	250	Aileu Complex	9.11	48.71	0.1130	0.511863	−15.0	−12.5	1.95
RIL169	300	Aileu Complex	8.63	44.82	0.1160	0.511872	−14.8	−11.9	1.99
RIL196	250	Aileu Complex	7.72	41.22	0.1130	0.511949	−13.3	−10.8	1.82
RIL228	250	Aileu Complex	6.71	34.58	0.1170	0.511877	−14.7	−12.3	2.00
TKI036	250	Aileu Complex	8.67	45.18	0.1158	0.512004	−12.3	−9.8	1.78
TKI066	250	Aileu Complex	9.03	44.43	0.1226	0.512109	−10.2	−8.0	1.74

340 Ma. Zircons within these populations are respectively characterised by U concentrations of 100–850 ppm and 85–1020 ppm, and mean Th/U of 0.76 and 0.85 (Fig. 5).

Two smaller age maxima each represent 12% of the data and yield mean ages of approximately 470 Ma and 1570 Ma. The 470 Ma population is defined by zircons with U concentrations between 130 and 660 ppm and a mean Th/U of 0.65. The 1570 Ma population is defined by zircons with similar U concentrations (210–620 ppm), but lower Th (30–230 ppm). Mean Th/U is consequently lower and equals 0.34 (Fig. 5). The final and modally least significant population, defined by 5% of the analysed zircon grains, has a mean age of 1770 Ma. These zircons are characterised by U concentrations and Th/U of 230–300 ppm and 0.52 respectively (Fig. 5). The remaining data defines a spread of ages between 600–1200 Ma and two older outliers with ages of 1900 Ma and 2520 Ma.

Zircons from sample LSP-111 are mostly colourless to yellow and show a CL response characterised by concentric oscillatory zoning. They are on average more rounded and smaller than those observed in sample LSP-079. Aspect ratios are typically 2:1 or less and grains are between 15 μm and 150 μm long. It was only possible to analyse forty-eight zircon grains for this sample, of which thirty-two analyses were concordant within the prescribed limits (Table 2). Given the smaller concordant dataset obtained from this sample, the probability of missing components of the detrital spectrum is higher. For example, the probability of missing a component of the age population constituting >10% of the total is 23% (Vermeesch, 2004).

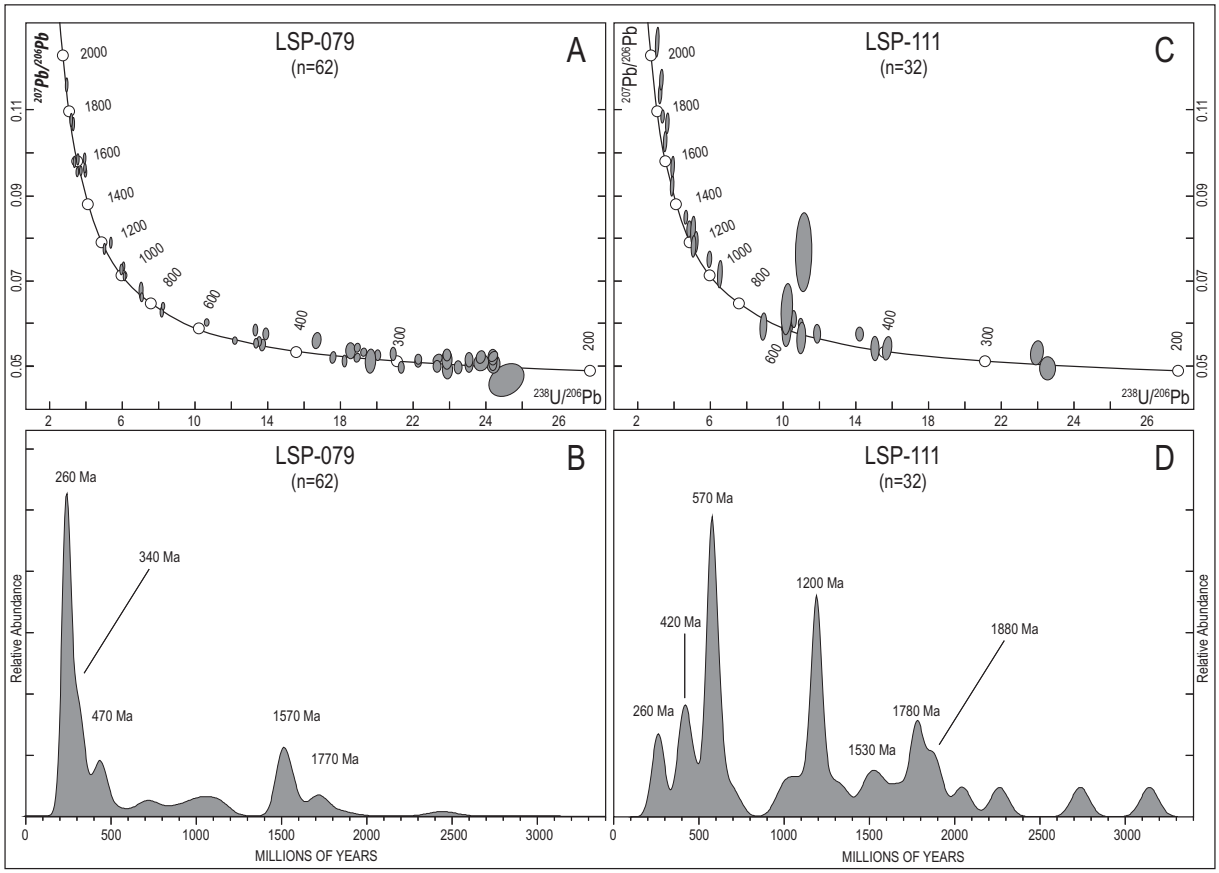

Fig. 4. U–Pb isotopic data for detrital zircons from the Gondwana Sequence. (A) Terra–Wasserburg plot of concordant U–Pb data for LSP–079. (B) Kernel density plot of concordant U–Pb data for sample LSP–079. (C) Terra–Wasserburg plot of concordant U–Pb data for LSP–111. Note: analyses 1 (2722 ± 13 Ma), 52 (3138 ± 15 Ma) and 63 (2260 ± 19 Ma) are outside the area of the diagram. (D) Kernel density plot of concordant U–Pb data for sample LSP–11. Kernel density plots are calculated using Densityplotter (Vermeesch, 2012) with adaptive input bandwidths.

Sample LSP-111 yielded ages between 260 Ma and 3140 Ma, with the majority <2000 Ma. The youngest two grains give a weighted mean $^{206}Pb/^{238}U$ age of 263 ± 2 Ma. This age is interpreted to define the maximum depositional age of this rock. The modally most significant age peak is defined by approximately 20% of the analysed grains. The zircons from this grouping are compositionally variable – U concentrations were 15–1150 ppm (mean = 310 ppm) and Th/U was 0.03–5.4 (mean = 1.3) – and yielded an age of 570 Ma (Figs. 4 and 5). The next most modally important age peak yielded an age of 1200 Ma and is defined by approximately 15% of the analysed grains. U concentrations for this grouping are between 60 ppm and 290 ppm and the mean Th/U = 0.43. Another five age peaks, each defined by between 5% and 10% of the analysed zircons, yielded ages of 260 Ma, 420 Ma, 1530 Ma, 1780 Ma and 1880 Ma. Mean U concentration and Th/U for each grouping is as follows: 260 Ma = 420 ppm and 0.7, 420 Ma = 520 ppm and 0.7, 1503 Ma = 200 ppm and 0.9, 1780 Ma = 380 ppm and 0.3, and 1880 Ma = 210 ppm and 0.7 (Fig. 5). Four outlying analyses yield older individual ages of 2104 Ma, 2260 Ma, 2730 Ma and 3140 Ma (Table 2).

5.2. Cluster analysis

To test the degree of similarity between our data and those published previously we have applied the kernel functional estimation method of Sircombe and Hazelton (2004). The calculated similarity relationships are illustrated in Fig. 6. The figure illustrates the hierarchical clustering of data whereby the samples with the most similar detrital zircon age spectra are paired. This pair is then treated as a single sample and the function estimate distance to the next most similar age spectrum is calculated. This process is continued until all samples have been merged.

The zircon age data from samples LSP079 and LSP111 are compared with those from samples KE133, KE342 (Ely et al., 2014) and 09HS21-4 (abbreviated here HS21; Spencer et al., 2016) from the Aileu Complex. We also include the data from sample TR8, river sand collected at the mouth of the Comoro River (Dinis et al., 2013), the headwaters of which fall entirely within the Aileu Complex. Samples from the Gondwana Sequence are BA6, BA12, BA21 from Kwon et al. (2014), sample EZ151 from Spencer et al. (2016), and samples TE11, TE14, SZ07, SZ17, SZ41, SZ48 and SZ49 from Zimmermann and Hall (2016).

Fig. 6 illustrates three broad groupings defined by between five and seven samples each. The first grouping (top grouping, Fig. 6) is characterised by a modally dominant 200–600 Ma age population together with a secondary Mesoproterozoic to Palaeoproterozoic (1450–1900 Ma) age population. The second grouping (middle grouping, Fig. 6) is also dominated by these two age groupings, although the Palaeozoic population is somewhat less dominant. The final grouping again contains the 200–600 Ma and 1450–1900 Ma populations, although for this grouping the 200–600 Ma age peak is broader and less unimodal, and an additional early Neoproterozoic to Mesoproterozoic (900–1250 Ma) age population is also present. Zircons of this age (900–1250 Ma) are generally either poorly developed or absent in the first two groupings.

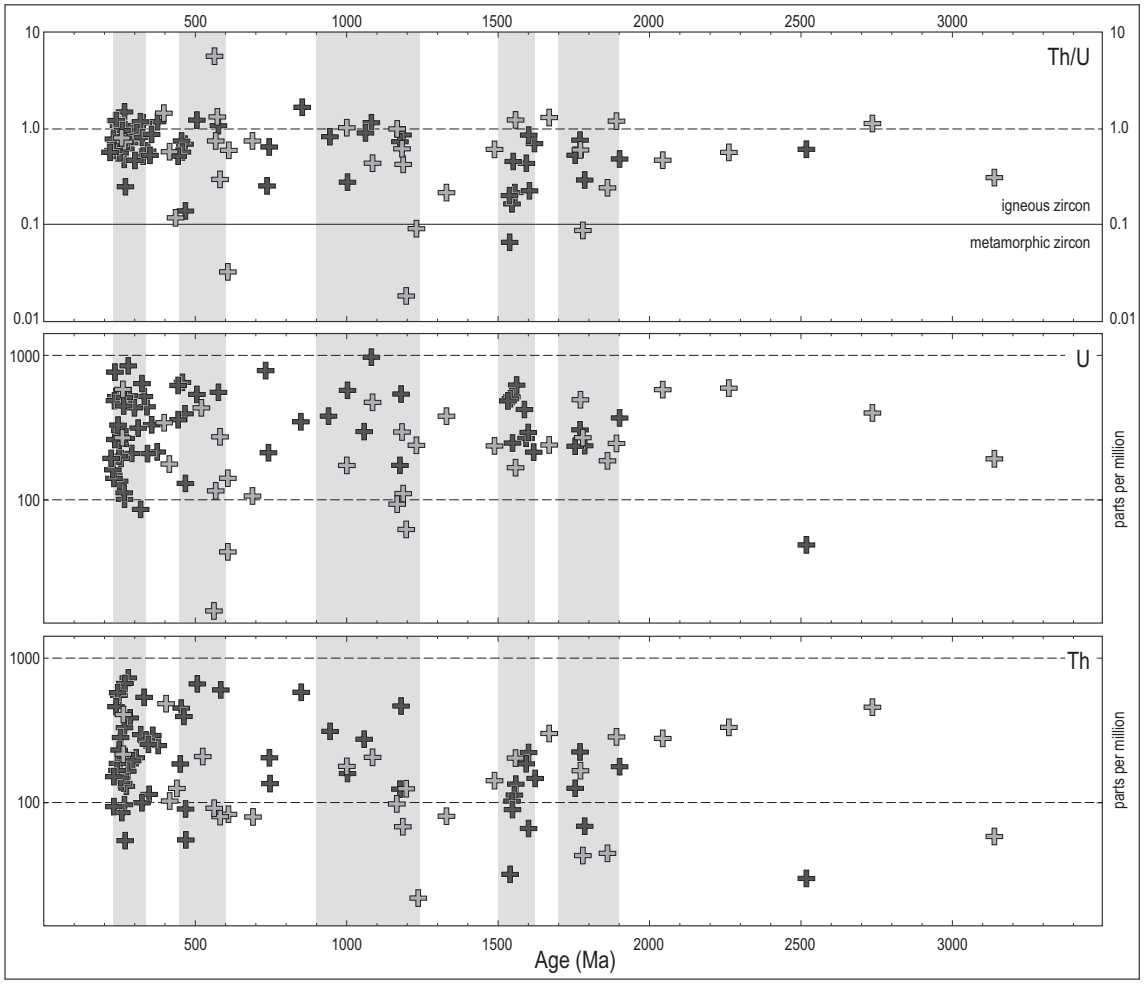

Fig. 5. Zircon U-Th compositional data. Dark grey crosses = sample LSP-079, middle grey crosses = sample LSP-111. Light grey bands highlight the main detrital populations. Note: (i) the general absence of metamorphic zircon (Th/U < 0.1) within the population, (ii) generally lower mean Th concentrations, and somewhat lower Th/U, in zircons >1500 Ma.

The results are interesting in the respect that: (1) the data from the Aileu Complex, although mostly concentrated in the third grouping, scatter across all three groups (Fig. 6) and, (2) data from widely distributed samples of the Niof and Babulu formations also scatter across all three groupings. Point (2) indicates that there appears to be no spatial or temporal trend in the detrital signatures observed for the Gondwana Sequence. The absence of a spatial trend is perhaps not surprising given that Timor is not a large island. However the spectral similarities observed for the Niof and Babulu formations (Zimmermann and Hall, 2016) imply both stable drainage pathways and/or source regions during at least the middle to late Triassic when these two formations were deposited.

The scattering of the samples from the Aileu Complex across all three groupings is also interesting and important as this is not what one would expect if the Aileu and Gondwana sequences were sourced from widely separated and unrelated source regions (Carter et al., 1976; Barber et al., 1977). If this were the case one would expect the samples from the Aileu Complex and the Gondwana Sequence to each show greater internally similarity when compared to samples from the other domain. Although there does appear to be a general trend whereby the rocks of the Gondwana Sequence are more commonly dominated by Phanerozoic aged zircon, samples from both sequences nevertheless show a large degree of overlap in their detrital spectra (Fig. 6). This is evident visually, but also confirmed statistically by the permutation (P) values given in the top right table of Fig. 6. This table illustrates that all samples are associated with several P values > 0.05. A P value > 0.05 indicates that the age distributions observed for that pair of samples is identical at a 2σ level. This implies that there is a strong thread of similarity for the age profiles from the Aileu Complex and the Gondwana Sequence, an observation that can be interpreted to suggest both sequences were likely derived from the same, or very similar source area.

Assuming a common provenance for the Gondwana and Aileu sequences, their source region was comprised of rocks with three major age peaks – 200–600 Ma, 900–1250 Ma and 1450–1900 Ma (Fig. 6). The youngest population is the most modally significant and is dominated by early to middle Permian aged zircon from which a modal age peak of c. 260 Ma can be resolved. A subordinate younger contribution to this population yields an early to middle Triassic age of c. 235 Ma, while the broad older side of this population can be unmixed to yield early Permian (c. 290 Ma), middle (c. 320 Ma) and early Carboniferous (c. 360 Ma), early Silurian (c.460 Ma) and Ediacaran (c. 590 Ma) age peaks. The 900–1250 Ma population is comprised of sub-populations with ages of c. 940 Ma, c. 990 Ma, c. 1060 Ma, c. 1160 Ma and c. 1210 Ma, while the 1450–1900 Ma population unmixes to yield sub-population modal age peaks at c. 1560 Ma, c. 1700 Ma, c. 1780 Ma and c. 1860 Ma.

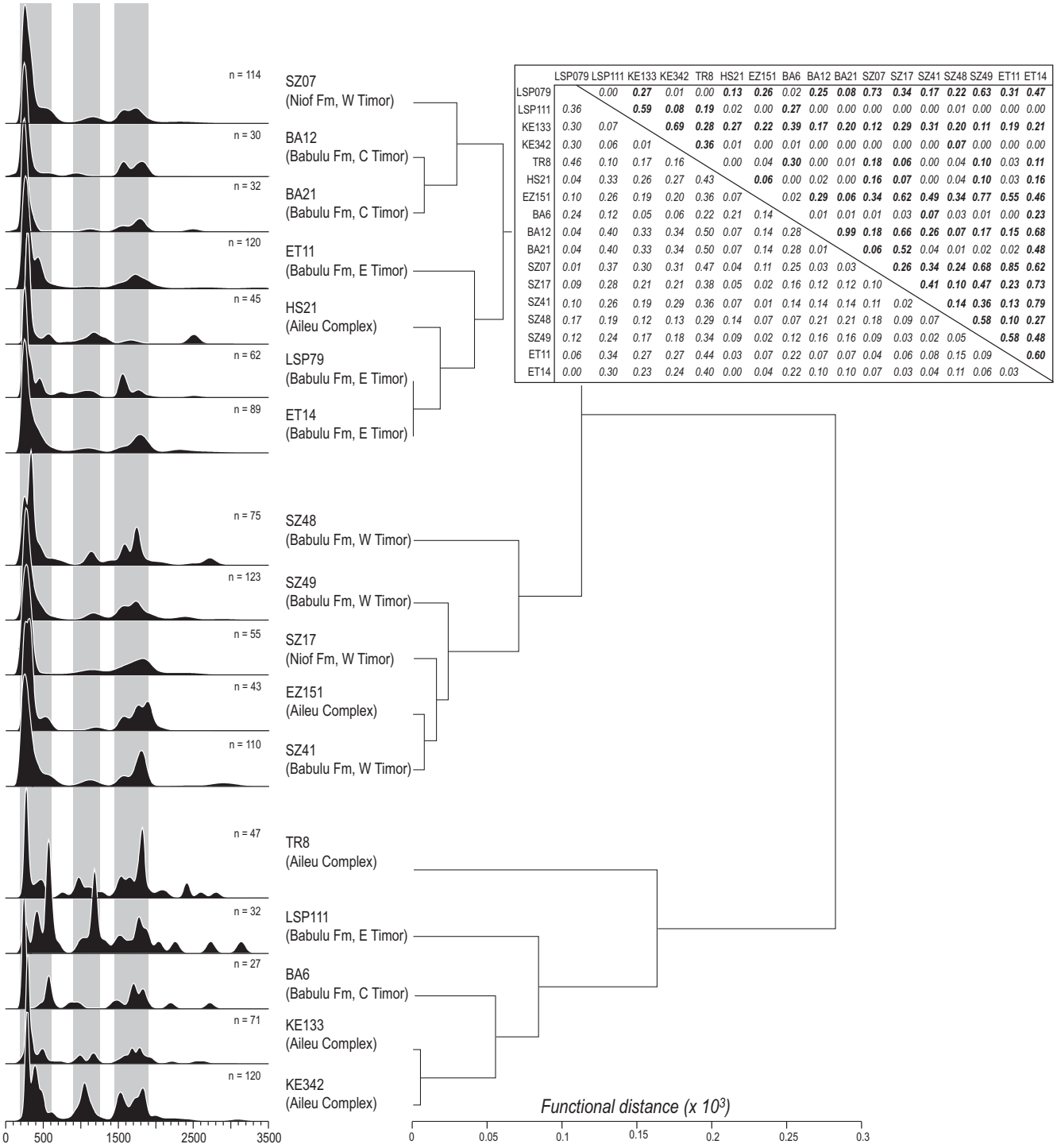

	LSP079	LSP111	KE133	KE342	TR8	HS21	EZ151	BA6	BA12	BA21	SZ07	SZ17	SZ41	SZ48	SZ49	ET11	ET14
LSP079		0.00	**0.27**	0.01	0.00	**0.13**	**0.26**	0.02	**0.25**	**0.08**	**0.73**	**0.34**	**0.17**	**0.22**	**0.63**	**0.31**	**0.47**
LSP111	0.36		**0.59**	**0.08**	**0.19**	0.02	0.00	**0.27**	0.00	0.00	0.00	0.00	0.00	0.01	0.00	0.00	0.00
KE133	0.30	0.07		**0.69**	**0.28**	**0.27**	**0.22**	**0.39**	**0.17**	**0.20**	**0.12**	**0.29**	**0.31**	**0.20**	**0.11**	**0.19**	**0.21**
KE342	0.30	0.06	0.01		**0.36**	0.01	0.00	0.01	0.00	0.00	0.00	0.00	0.00	**0.07**	0.00	0.00	0.00
TR8	0.46	0.10	0.17	0.16		0.00	0.04	**0.30**	0.00	0.01	**0.18**	**0.06**	0.00	0.04	**0.10**	0.03	**0.11**
HS21	0.04	0.33	0.26	0.27	0.43		**0.06**	0.00	0.02	0.00	**0.16**	**0.07**	0.00	0.04	**0.10**	0.03	**0.16**
EZ151	0.10	0.26	0.19	0.20	0.36	0.07		0.02	**0.29**	**0.06**	**0.34**	**0.62**	**0.49**	**0.34**	**0.77**	**0.55**	**0.46**
BA6	0.24	0.12	0.05	0.06	0.22	0.21	0.14		0.01	0.01	0.01	0.03	**0.07**	0.03	0.01	0.00	**0.23**
BA12	0.04	0.40	0.33	0.34	0.50	0.07	0.14	0.28		**0.99**	**0.18**	**0.66**	**0.26**	**0.07**	**0.17**	**0.15**	**0.68**
BA21	0.04	0.40	0.33	0.34	0.50	0.07	0.14	0.28	0.01		**0.06**	**0.52**	0.04	0.01	0.02	0.02	**0.48**
SZ07	0.01	0.37	0.30	0.31	0.47	0.04	0.11	0.25	0.03	0.03		**0.26**	**0.34**	**0.24**	**0.68**	**0.85**	**0.62**
SZ17	0.09	0.28	0.21	0.21	0.38	0.05	0.02	0.16	0.12	0.12	0.10		**0.41**	**0.10**	**0.47**	**0.23**	**0.73**
SZ41	0.10	0.26	0.19	0.29	0.36	0.07	0.01	0.14	0.14	0.14	0.11	0.02		**0.14**	**0.36**	**0.13**	**0.79**
SZ48	0.17	0.19	0.12	0.13	0.29	0.14	0.07	0.07	0.21	0.21	0.18	0.09	0.07		**0.58**	**0.10**	**0.27**
SZ49	0.12	0.24	0.17	0.18	0.34	0.09	0.02	0.12	0.16	0.16	0.09	0.03	0.02	0.05		**0.58**	**0.48**
ET11	0.06	0.34	0.27	0.27	0.44	0.03	0.07	0.22	0.07	0.07	0.04	0.06	0.08	0.15	0.09		**0.60**
ET14	0.00	0.30	0.23	0.24	0.40	0.00	0.04	0.22	0.10	0.10	0.07	0.03	0.04	0.11	0.06	0.03	

Fig. 6. Detrital zircon age spectra and functional distance dendrogram for samples from the Aileu Complex and the Gondwana Sequence. Left hand column shows age kernel density plots with the number of concordant analyses given in the top right of each plot. Table upper right show the calculated matrix of comparison (Sircombe and Hazelton, 2004) on which the dendrogram is based. Values in the lower left half of the matrix are the calculated functional estimate distances ($\times 10^3$). The values in the upper right half are permutation values for testing the equality of age distributions. Values highlighted in bold font are those for which the two samples have statistically identical age profiles within 2σ confidence limits.

5.3. Major and trace element geochemistry

Mudstones, phyllities and schists of the Aileu Complex have SiO_2 concentrations between 58 and 71 wt%, with a mean of 65 wt% (Table 3). Of the sixteen analysed samples from this formation, thirteen are high-SiO_2 type (SiO_2 > 63 wt%). Potassium and sodium concentrations are 2.5–4.6 wt% and 0.9–3.0 wt%, with mean values of 3.8 wt% and 1.5 wt% respectively (Table 3). K_2O/Na_2O and Mg# (MgO/(MgO + FeO)) average 3.1 and 0.26, and TiO_2 concentrations range between 0.64 and 0.78, with a mean of 0.72.

By comparison, the mudstones from the Gondwana Formation are notably less siliceous and potassic, but more ferruginous (Fig. 7). For these rocks SiO_2 concentrations range between 56

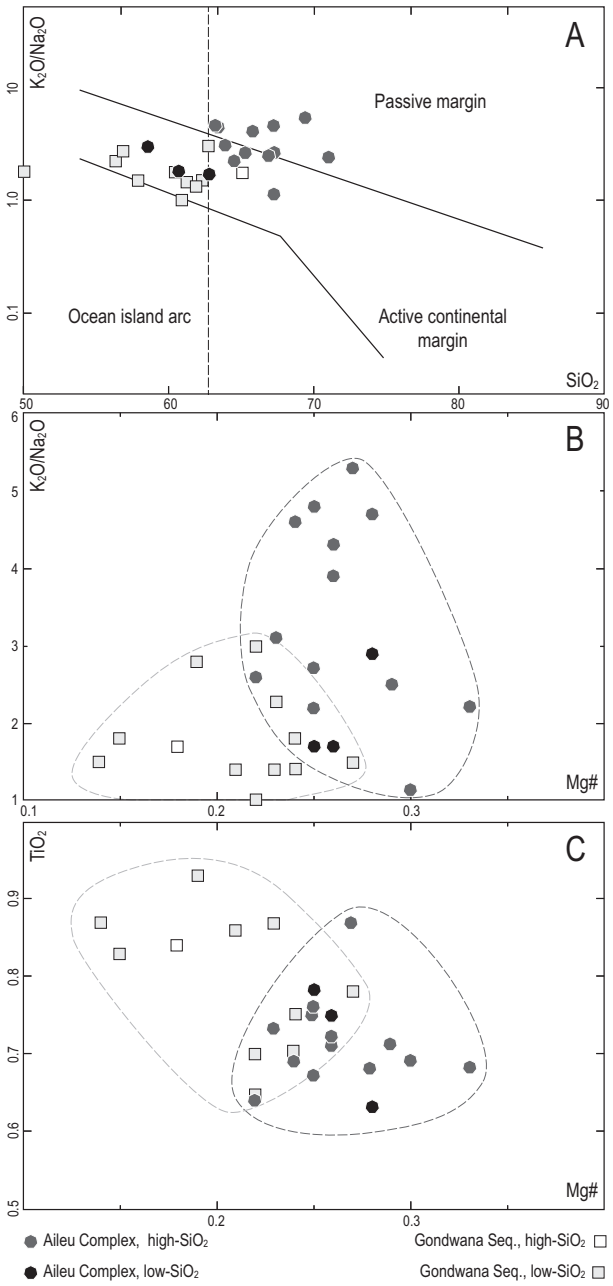

Fig. 7. Whole rock geochemical data for argillitic sediments the Aileu Complex and Gondwana Sequence. (A) SiO_2 verse K_2O/Na_2O discrimination plot of Roser and Korsch (1986). (B) Mg# verse K_2O/Na_2O. (C) Mg# verse TiO_2. For plot (C), note that sample OLI040 (Gondwana Sequence) plots outside of the field of view. For both (B) and (C) the dark grey dashed line encloses analyses from the Aileu Complex, the light grey dashed line encloses analyses from the Gondwana Sequence. Note the limited overlap between these fields.

and 65 wt% with a mean of 60 wt% (Table 4). Only one of the thirteen samples from this sequence classifies as high-SiO_2 type. The mean FeO and TiO_2 concentrations are 7.0 wt% and 0.76 wt% (Table 4) and compare to mean values of 5.5 wt% and 0.72 wt% for the Aileu Complex (Table 3). Part of this difference may be due to the lower mean concentrations of SiO_2, although this can only partly explain the difference as Mg# is lower (mean = 0.21) in the Gondwana Sequence than in the Aileu Complex (mean = 0.26). K_2O and N_2O are also present in respectively lower and higher abundances in the mudstones of the Gondwana Sequence when compared to those of the Aileu Complex. K_2O/Na_2O is therefore lower and yields a mean value of 1.8 (Table 4), which compares to a mean of 3.1 for the Aileu Complex. Calcium concentrations are also on the whole higher and more variable in the Gondwana Sequence (mean = 2.7 wt%).

Although there is some overlap, argillites from the Aileu Complex differ compositionally from those of the Gondwana Sequence. They plot higher and to the right of the rocks from the Gondwana Sequences in the SiO_2 verse K_2O/Na_2O diagram, and fall within the active continental and passive margin fields on this plot (Fig. 7). In contrast, the rocks of the Gondwana Sequence fall mostly within the active continental margin field. These differences are also apparent on the K_2O/Na_2O verse Mg# and TiO_2 verse Mg# plots illustrated in Fig. 7b and c. These plots both show a high degree of compositional separation between the Aileu and Gondwana sequences.

Rare earth element (REE) patterns for both the Aileu and Gondwana sequences are similar and are characterised by light (L)REE enrichment relative to heavy (H)REE, a flat trend between middle (M)REE and HREE, and a negative Eu anomaly (Fig. 8). The absolute abundance of REE for the Aileu Complex is somewhat higher, although the normalised trends are very similar. The ratios $(La/Lu)_N$, $(Gd/Lu)_N$ and Eu/Eu^* equal 9.8, 1.6 and 0.6 for the Aileu Complex, and 9.0, 1.2 and 0.6 for the Gondwana Sequence. These characteristics are common to typical post-Archaean shales (Taylor and McLennan, 1985).

Although the REE patterns of these two sequences are similar, the differences apparent in the whole rock data reappear when one considers the abundances of the provenance sensitive trace elements. The elements Ti, Sc, V, Ga and Na are associated with mafic volcanic lithic grains and their concentration in clastic sediments is interpreted to reflect the input of island and continental arc material (Bhatia and Crook, 1986; McLennan et al., 1990). Conversely, LREE, Rb and the highly charged cations Th, U, Nb, Zr and Hf reflect high abundances of mica and the heavy minerals zircon, monazite, tourmaline and rutile. These minerals generally reflect the input of granitic or recycled continental crust (Bhatia and Crook, 1986; McLennan et al., 1990).

Th/Sc is used to measure the relative input of arc to continental material and, for the Aileu Complex this ratio varies between 1.0 and 2.1 with a mean of 1.5. These values compare to a range of 0.8–1.2 and a mean of 0.9 for the Gondwana Sequence. When plotted on the Th–Sc–Zr ternary diagram the data from the Gondwana Sequence plots almost entirely in the continental island arc (CIA) field, whereas the data from the Aileu Complex falls mostly within the active continental margin (ACM) field (Fig. 8).

Other provenance sensitive trace element ratios also show a consistent shift from more continental-like compositions for the mudstones of the Aileu Complex, to more arc-like compositions for the Gondwana Sequence. On a plot of Rb/Sr against Th + U, the rocks from the Aileu Complex plot in a wide scatter in the upper right in this diagram and separate completely from those of the Gondwana Sequence (Fig. 8d). Both Rb/Sr and the concentrations of Th and U increase with more felsic and continental (and mature) source rocks given the greater input from detrital mica, zircon and monazite. In contrast Sr is a proxy for plagioclase, the primary feldspar in mafic rocks. Ba, which substitutes for K in alkali feldspar, and the LREE La are relatively enriched in granitic rocks when compared to Ti, Cr and Ni, which are all higher in mafic and ultramafic rocks. The ratios Ba/Ti and La/(Cr + Ni) thus both increase with more felsic source rocks. Similar to the plot of Rb/Sr against Th + U, the rocks from the Aileu Complex scatter in the upper right quadrant of a plot of La/(Cr + Ni) verse Ba/Ti and show very little compositional overlap with the samples from the Gondwana Sequence (Fig. 8e).

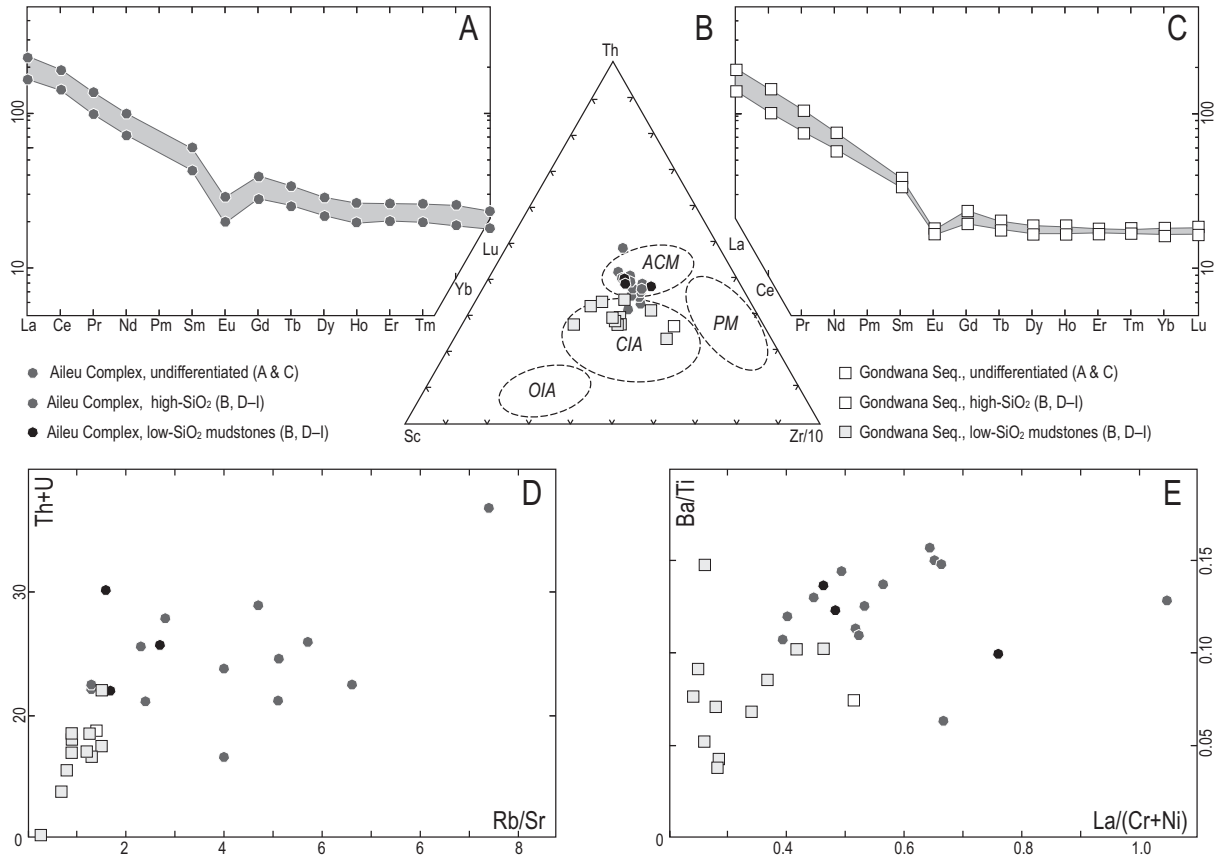

Fig. 8. Trace element and rare earth data for the Aileu and Gondwana sequences. (A) Chondrite normalised REE spiderdiagram for Aileu Complex argillites. (B) Ternary Sc–Th–Zr/10 discrimination plot of Bhatia and Crook (1986). Fields are: ACM = active continental margin, CIA = continental island arc, OIA = Ocean island arc and PM = passive margin. (C) Chondrite normalised REE spiderdiagram for Gondwana Sequence argillites. Normalising factors for (A) and (C) are after Sun and McDonough (1989). (D–E) Bivariant trace element plots illustrating the limited compositional overlap between the Aileu Complex and the Gondwana sequence.

5.4. Nd isotope geochemistry

Sm–Nd abundances and measured $^{147}Sm/^{144}Nd$ and $^{143}Nd/^{144}Nd$ are presented in Table 7. For the Aileu Complex, Sm and Nd concentrations vary between 4–12 ppm and 23–62 ppm. Measured values for $^{147}Sm/^{144}Nd$ vary between 0.1130 and 0.1226, while $^{143}Nd/^{144}Nd$ varies between 0.51180 and 0.51211. Present day εNd for the mudstones, phyllites and schists of the Aileu Complex is between −10.2 and −16.2, while $\varepsilon Nd_{(250)}$ (where $\varepsilon Nd_{(250)}$ = the initial εNd calculated at the time of sediment deposition – c. 250 Ma) varies between −8.1 and −13.9 (mean = −12.0). Applying the linear mantle evolution curve of Goldstein et al. (1984), the Nd T_{DM} model ages for Aileu Complex argillites vary between 1.7 Ga and 2.1 Ga (Table 7).

For the Gondwana Sequence, the Sm and Nd abundances vary between 3–10 ppm and 20–50 ppm. $^{147}Sm/^{144}Nd$ (0.0851–0.1240) is more hetrogeneous than for the Aileu samples, and $^{143}Nd/^{144}Nd$ (0.51203–0.51231) is higher. Present day εNd and $\varepsilon Nd_{(230Ma)}$ vary from −6.3 to −11.7 (mean = −9.2) and from −4.0 to −9.0 (mean = −6.7), while the Nd T_{DM} model ages for the Gondwana Sequence are between 1.3 Ga and 1.7 Ga.

Gondwana Sequence argillites thus have systematically higher (less negative) εNd and younger model ages than those of the Aileu Complex. These data indicate that the Gondwana Sequence was sourced from an isotopically more juvenile source, consistent with the geochemical data that suggest a more mafic and arc-like source for these rocks. The differences between the two sequences are illustrated in Fig. 9, which plots Nd T_{DM} model age against Th/Sc. The figure illustrates a complete isotopic and geochemical separation between the two sequences.

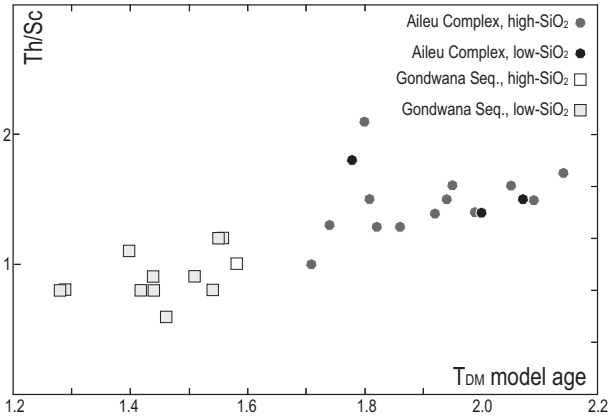

Fig. 9. T_{DM} model age verse Th/Sc plot for the Aileu Complex and Gondwana Sequence. Note the complete compositional separation of the two sequences.

6. Discussion

6.1. Provenance implications from detrital zircon data

The U-Pb detrital zircon age data collected here are consistent with detrital zircon datasets reported in previous studies. When

combined, these datasets collectively suggest that the Aileu Complex and the Gondwana Sequence have very similar detrital zircon age distributions with major age components at 200–600 Ma, 900–1250 Ma and 1450–1900 Ma. The youngest grouping (200–600 Ma) is modally most significant and contains a dominant age mode at c. 260 Ma.

Two contrasting views have been presented regarding the likely origin of these zircons. Ely et al. (2014) identified the Sula Spur, the northern and along strike continuation of the active Pacific margin of Pangaea (Fig. 10), as a possible source. The Sula Spur was also implicated as a possible source for the Triassic zircon ages by Dinis et al. (2013), Spencer et al. (2016) and Zimmermann and

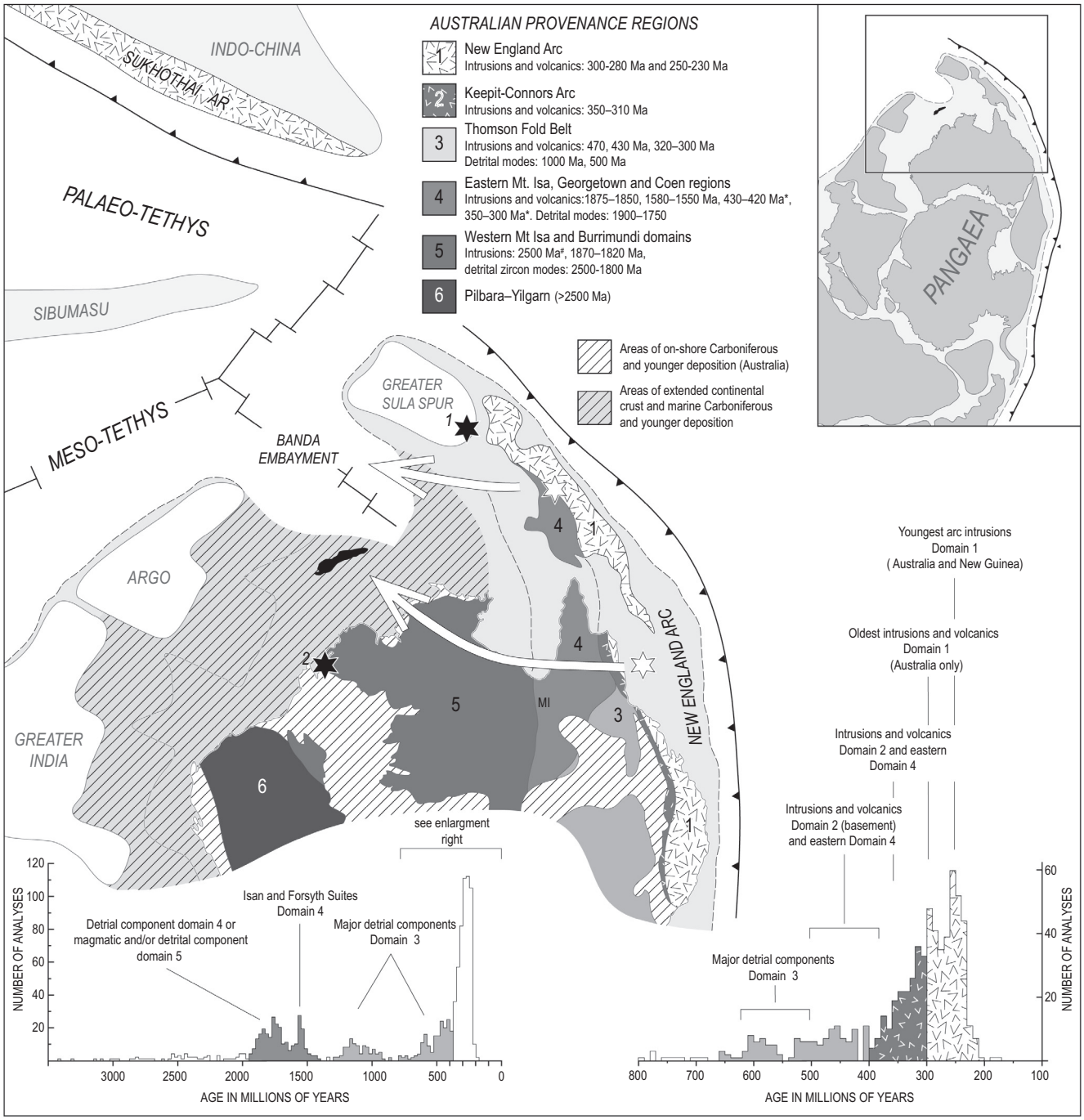

Fig. 10. Tectonic cartoon of northern Pangaea in the early Triassic (c. 250 Ma). The figure is drawn after the reconstructions of Charlton (2001), Harrowfield et al. (2005), Hall et al. (2012) and Metcalfe (2013b). Inset top right illustrates the location of the main figure within Pangaea. The histograms at the bottom of the figure show the combined zircon age distribution for the Aileu and Gondwana sequences. Histograms are constructed from the concordant data presented in this study, combined with data from Dinis et al. (2013), Ely et al. (2014), Kwon et al. (2014), Spencer et al. (2016) and Zimmermann and Hall (2016). Colour coding of the histogram, figure and legend shows the possible sources for the obtained detrital zircon ages. Stars mark inferred source regions. Black stars are after: (1) Ely et al. (2014) and (2) Harris (2006), white stars are for this study. White arrows mark speculative sediment transport paths. Upper arrow = Aileu Complex, lower arrow = Gondwana Sequence. Note: we do not imply specific source locations, only that the Aileu and Gondwana sequences are likely derived from different parts of the active eastern margin of Pangaea. In the legend, asterisk (∗) = Georgetown and Coen regions (east) only and hash (#) uncommonly exposed basement. MI = Mt Isa. Note: boundary between domains 3 and 4 defines the "Tasman Line" and marks the boundary between the Proterozoic and Phanerozoic rocks in eastern Australia.

Hall (2016), although these studies also argued that the Palaeoproterozoic component of the detrital spectrum was likely derived from the basement of north-western Australia, a hypothesis championed by Harris (2006). By contrast Harris (2006) attributed the Mesozoic zircons to magmatism associated with the break-up and northward drift of crustal blocks from northern Pangaea, implying a proximal source located near to north-western Australia.

Although Palaeoproterozoic zircon ages (particularly those with ages between 1800 and 1900 Ma) in the Timorese sediments can be matched with the age of the basement rocks exposed in north-western Australia, we do not consider this region to be a very likely source for the sediments of the Gondwana and Aileu sequences. The reason for this conclusion is twofold.

Firstly, the northwest of Australia was a site of widespread sediment deposition during the late Palaeozoic and Mesozoic (Eyles et al., 2002; Mory et al., 2008). This implies that this region was low-lying and recieving sediment at the same time as deposition was occuring in Timor. The widespread preservation of Carboniferous and younger strata (Fig. 10) further suggests that there has been limited post-depositional uplift and denudation and, where denudation has occurred, thermochronologic data tend to support the inference that much of what was stripped away was Palaeozoic sediment, rather than the presently exposed basement (Gleadow et al., 2002). In our view, these factors limit the extent to which the Palaeoproterozoic basement in this area could have contributed to the Aileu and Gondwana sequences.

Secondly, the dominance of Permo-Triassic aged zircon in the Timorese sediments (Fig. 5) implies a source region dominated by Permo-Triassic rocks. Geochemical data presented here also indicate an active convergent plate margin source, a conclusion supported by the overlap in depositional age and the dominant detrital zircon mode (Cawood et al., 2012). With these points in mind, we consider it more likely that either the Sukhothai and New England arcs represent the dominant source for the Aileu and Gondwana sequences (Fig. 9). Both arcs were active at the appropriate time, were proximal to northeast Pangaea during the Permo-Triassic, and would provide detritus with the right geochemical and isotopic characteristics.

The Sukhothai Arc is exposed in the central and eastern Malay Peninsula and extends north-northwest into central Thailand (Metcalfe, 2013a). Arc magmatism was related to subduction beneath the northern margin of the Indochina block, an event that coincided with the rifting of the Sibumasu Block from the north margin of Pangaea (Fig. 10). Magmatism in the Sukhothai arc occurred in two closely spaced pulses, between 270–230 Ma and 220–200 Ma (Searle et al., 2012).

The New England arc represents the youngest phase of a long-lived period of plate convergence and accretionary growth that occurred along the eastern palaeo-Pacific margin of Pangaea. This process began in the Cambrian when subduction initiated along the outboard Pacific margin of the newly formed Gondwana supercontinent (Boger and Miller, 2004; Foden et al., 2006). Thereafter plate convergence quasi-continuously up-scraped and accreted continental derived sediment, or sutured arc derived magmatic and sedimentary rocks, to the east Gondwana, then later Pangaea, margin (Cawood, 2005; Cawood and Buchan, 2007; Pankhurst and Vaughan, 2009; Boger, 2011). The New England Arc is exposed between Sydney and Townsville along the northeast coast of Australia (Fig. 10). It is inferred to continue along strike to the north into New Guinea, while the southern and rifted extension of this orogen extends to at least the Lord Howe Rise and may be present in New Zealand (Muir et al., 1998; Charlton, 2001; Van Wyck and Williams, 2002; Crowhurst et al., 2004; Mortimer et al., 2008; Tulloch et al., 2009; Cawood et al., 2011).

The Permo-Triassic phase of the New England Arc is built upon the late Devonian to Carboniferous (360–305 Ma) Keepit-Connor Arc (Fig. 9). The magmatic expression of the Keepit-Connor Arc intrudes both the adjacent Thomson Fold Belt and the Palaeoproterozoic basement of the Georgetown Inlier. This event also dispersed large volumes of volcanogenic sediment into adjacent forearc basins (Black and McCulloch, 1990; Roberts et al., 1995; Allen et al., 1998; Bryan et al., 2004; Murgulov et al., 2013). Keepit-Connor arc magmatism was terminated by a short period of compressional deformation dated to 305–295 Ma, which was immediately followed by voluminous bimodal volcanism and the coeval emplacement of granitoid intrusions associated with the New England Arc. Magmatism occurred between 295 Ma and 275 Ma and was followed by Hunter-Bowen orogenesis. This event occurred at approximately 265 Ma and was followed by a renewed pulse of arc magmatism that lasted from 250 Ma until 230 Ma (Roberts et al., 1996; Jenkins et al., 2002; Offler and Foster, 2008; Korsch et al., 2009a, 2009b; Cawood et al., 2011; Rosenbaum et al., 2012).

Of these two arc systems, the Sukhothai Arc can probably be excluded as a viable source for the Aileu and Gondwana sediments. When active, the Sukhothai Arc was separated from the Pangaean plate by the Palaeo- and Meso-Tethys Oceans (Fig. 10). North directed subduction beneath the Sukhothai Arc would additionally have ensured that south flowing arc-derived sediment was likely accreted into the forearc accretionary prism, leaving little chance for this material to be transferred tectonically to the Pangaean plate. In contrast, one can easily conceive a source to sink relationship between continental arc magmatism along the eastern seaboard of Pangaea and sedimentation on the passive northwestern side of this plate (Fig. 10).

Assuming this scenario is correct – that the Timorese sediments were derived from the eastern active margin of Pangaea – one might expect these rocks to contain zircons that reflect New England arc magmatism, but also the basement to the arc, and rocks that were present in the immediate forearc. A comparison of the geology of the eastern Australia with the detrital zircon spectrum observed in the Timorese sedimentary rocks, suggests this is indeed the case.

Within the Aileu and Gondwana sequences the modally most significant age population yields ages between 200 and 600 Ma. Unmixing of this population yields a major age mode at approximately 260 Ma, but also sub-populations of c. 235 Ma, c. 320 Ma, c. 360 Ma, c. 460 Ma and c. 590 Ma (Fig. 9). The c. 260 Ma population closely corresponds with Hunter-Bowen orogenesis within the New England Arc, while both the slightly older and younger sub-populations can be related to magmatic activity associated with the Keepit-Connor Arc (360–305 Ma) and the youngest Hunter-Bowen phase of the New England arc (250–230 Ma). Ages between 500 and 400 Ma correspond to both pre-tectonic granite emplacement and the coeval extrusion of volcanic rocks, as well as subsequent upper-amphibolite facies metamorphism observed within the northern Thomson Fold Belt (Withnall et al., 1991; Nishiya et al., 2003; Fergusson et al., 2007a, 2007b). The plutonic and volcanic expression of this event is also found in the immediately adjacent regions west of the Tasman line (Black and McCulloch, 1990; Hutton et al., 1997). The oldest age devolved from the 200 to 600 Ma population (580 Ma), together with the entire 900–1250 Ma population can be found as the dominant detrital components within the Palaeozoic sedimentary rocks of the Thomson Fold Belt (Fergusson et al., 2001, 2007a).

The final major age component found within both the Aileu Complex and the Gondwana Sequence (1450–1900 Ma) and can be unmixed to reveal sub-populations with modal age peaks at 1560 Ma, 1700 Ma, 1780 Ma and 1860 Ma. The 1560 Ma age peak corresponds with the age of the Forsyth batholith and the

cogenetic Croydon Volcanics, rocks that are exposed widely in the Georgetown and Coen regions immediately west of the Thomson Fold Belt in northern Australia (Black and McCulloch, 1990; Blewett et al., 1998). Rocks of equivalent age are also exposed as far west as the eastern parts of the Mt Isa Inlier (Page and Sun, 1998; Betts et al., 2006). In both areas this event was accompanied by mid- to high-temperature metamorphism and the growth of new zircon (Page and Sun, 1998; Giles and Nutman, 2002; Black et al., 2005).

The modal age peaks at 1700 Ma, 1780 Ma and 1860 Ma are found as both granitic and felsic volcanic basement to the sedimentary successions of the Mt Isa Inlier, and as the dominant detrital zircon modes within the sedimentary successions. The basement of the Mt Isa region is defined by the 1875–1850 Ma Kalkadoon and Ewen Batholiths and their coeval felsic volcanic rocks. The overlying cover rocks divide into two sequences that were deposited between 1800 and 1600 Ma and which contain, as their dominant detrital zircon component, zircons with ages between 1900 Ma and 1750 Ma (Neumann et al., 2006, 2009).

Ages between 1900 and 1750 Ma are not unique to the Mt Isa and Georgetown regions, but are almost universally present in Palaeoproterozoic sedimentary rocks (domain 5, Fig. 9) exposed in northern and central Australia (Claoué-Long et al., 2008a, 2008b; Rösel et al., 2014). However, sedimentary rocks west of Mt Isa increasing slow a secondary age peak at approximately 2500 Ma, an age which is poorly represented in the Aileu or Gondwana Sequences. For this reason we infer that the majority of the detritus for the Aileu and Gondwana sequences was likely derived from eastern Pangaea, with little input from north-central and northwest Australia. This is consistent with the geochemistry and Nd isotopic systematics which show affinities to an active continental margin (Figs. 7 and 8).

Although derivation of the Aileu and Gondwana sequences from the active eastern margin of Pangaea appears likely, we note that in many cases the magmatic products of this arc have notably higher εNd and younger Nd T_{DM} model ages than the Aileu and Gondwana sequences. For example, the components of the late Carboniferous to early Triassic New England batholith typically yield εNd values between −2.0 and +8 and Nd T_{DM} model ages <1.0 Ga (Hensel et al., 1985; Caprarelli and Leitch, 1998). The Nd isotopic systematics of the New England arc do however vary both along and across strike. More evolved rocks are present in northern Queensland (Hodgkinson Province) and, in this area, there is also a systematic decrease in εNd from east to west as these rocks intrude progressively older basement (Champion and Bultitude, 2013). εNd values range between −6.5 and −2.0 in the east and between −7.0 and −15.0 in the west (Champion and Bultitude, 2013). Equivalent T_{DM} model ages are between 1.2–1.5 Ga (east) and 1.3–2.0 Ga (west), values that overlap more closely with those observed in the Aileu and Gondwana sequences (Table 7). Part of the difference in isotopic character observed between the intrusive rocks of the New England arc and the sedimentary strata in Timor will also be a function of the degree of mixing of older crustal rocks. This is evident from the detrital age spectum that, although dominated by Permo-Triassic zircon, also contains a range of older grains.

6.2. Provenance implications from geochemical and isotopic data

Although the detrital zircon data support an east Pangaean provenance for the Aileu and Gondwana sequences, we cannot specify from where along this arc these sediments were derived. Our results do not for example preclude northern New Guinea and the Sula Spur as a possible source area (Ely et al., 2014; Zimmermann and Hall, 2016), although nor can we exclude sections of the arc exposed further to the south. Our geochemical and isotopic data highlight systematic compositional differences between the Gondwana and Aileu sequences—rocks from the Gondwana Sequence are compositionally more mafic, show lower K_2O/Na_2O, Rb/Sr, Th/Sc (Figs. 7 and 8) and yield markedly younger Nd model ages (Fig. 9) when compared to the rocks of the Aileu Complex. This outcome implies that the provenance history of these sequences is likely to be more complex than is suggested by the zircon data alone.

There are perhaps two ways to explain the isotopic and geochemical differences observed for the Gondwana and Aileu sequences. One option would be to imply that these geochemical differences result from temporal differences in the timing of deposition of these two sequences. In this scenario the temporal geochemical evolution of the arc, or perhaps the climatic history of northern Pangaea, is mirrored by changes in the compositions of the sediments. The alternate solution is spatial. In this case one would assume that the Aileu and Gondwana sequences have overlapping depositional ages, but were sourced from different parts of the arc that either exposed compositionally different rocks, exposed similar rocks but in differing proportions, or exposed the same rocks but these were exposed in differing climatic zones, which induced differing degrees of chemical weathering en route to their ultimate point of deposition.

In our view the temporal option is not satisfactory because the deposition of the Gondwana and Aileu sequences appears to largely overlap (Brunnschweiler, 1978; Barber et al., 1977; Carlton, 2002, 2009; Dinis et al., 2013; Davydov et al., 2013; Haig et al., 2014; Ely et al., 2014). Given the breadth and density of our sampling we also believe we are likely to have sampled rocks from a range of stratigraphic levels within each sequence. Despite this, our analytical data remain remarkably coherent for each sequence. We take this to suggest that the chemistry of these rocks is unlikely to be a phenomenon related to temporal changes in sediment source, but rather a long-lived feature inherent to each sequence. On this basis we imply a spatial control on the observed differences in chemistry.

To clarify the scale at which we think this spatial control may have operated, consider modern South America as an analogue for the north-eastern margin of Pangaea. The Andean arc is approximately the same length as the section of the east Pangaean margin of interest. Both arcs trend approximately north-south and have long drainage networks that feed/fed detritus from a continental arc to the passive side of the continent (Fig. 11).

The northern and central Andean highland is drained by three basins; the Amazon, La Plata and Magdalena basins (Fig. 11). These vary in surface area from between 250,000 km^2 to >6,000,000 km^2 and drain to widely separated (>1000 km) outlets (Lehner et al., 2006). As the continent narrows to the south, the drainage basins reduce in surface area, sample progressively smaller sections of the arc, and deposit their sedimentary load closer together. The composition of the sediments observed along the eastern coast of South America varies, but in a remarkably systematic fashion. They can be divided into three broad associations: Andean, Brazilian and Transitional (Potter, 1994).

The Andean association is defined by lithic arenite type sediments in which Q:F:Rf (Quartz:Feldspar:Rock fragment) and Fp/Ft ($plag_{mode}/(plag_{mode} + ksp_{mode})$ ratios equal approximately 33:15:52 and 0.73 (Potter, 1994). This association includes: (i) all sediment derived from the Andean highland and transported to the Pacific coast, (ii) sediment transported to the northern Atlantic coast within the Magdalena Basin and, (iii) sediment derived from all rivers south of and including the La Plata River (Fig. 11).

The Brazilian association accounts for sediments derived mostly from the continental Brazilian and Guyanan highlands with little direct input from the Andean arc. These sediments are transported by low relief tropical streams and are compositionally mature. Q:F:Rf and Fp/Ft values 86:7:7 and 0.27. This grouping accounts for all

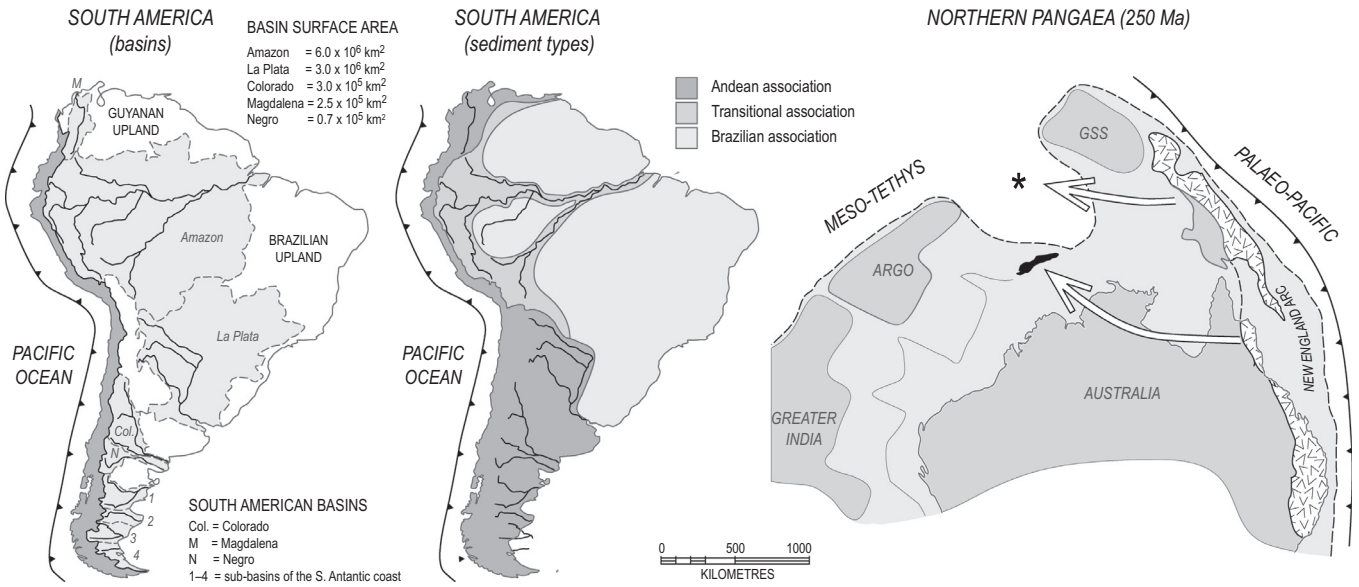

Fig. 11. Comparison of modern South America and Permo-Triassic northern Pangaea. Figure left shows the major present day drainage basins of South America. Areas coloured dark grey drain from the Andean highlands to the Pacific Ocean. Areas coloured middle grey are basins that drain from the Andean highlands to the Atlantic margin (i.e. drainage systems most similar to those which transported sediment from the east Pangaean highlands to the basins in which the Gondwana and Aileu sequences of Timor were deposited). Areas coloured white are those which are either internally drained or which drain to the Atlantic Ocean with no connection to the Andean Highlands. Figure centre shows the distribution of major sediment types in South America (after Potter, 1994). The Andean association is compositionally most like the Gondwana Sequence (lowest SiO_2, lowest K_2O/NaO_2), while the transitional association is compositionally most similar to the Aileu Complex (strong arc affinities but higher SiO_2 and K_2O/NaO_2). Figure right is the reconstruction of northern Pangaea in the Permo-Triassic with Timor marked black. The Pangaean highlands are defined by the New England Arc. White arrows are speculative sediment transport paths. Upper arrow = Aileu Complex, lower arrow Gondwana Sequence. Asterisk (∗) marks the proposed location of deposition of the Aileu Complex. GSS = Greater Sula Spur. All images are drawn to the same scale.

sediment found along the Atlantic coast between the Magdalena Basin and the mouth of the La Plata River, with the exception of the sediment found at the mouth of the Amazon River (Potter, 1994).

Intermediate between these two families is the Transitional association. These sediments are found in the headwaters of the Amazon River adjacent to the Andes and along the trunk flow of the Amazon River where the volume and speed of transport preclude appreciable in situ weathering (Fig. 11). This allows for the transport of Andean type petrographic signatures to the Atlantic Ocean, albeit with some mixing with detritus from the cratonic Brazilian and Guyanan sources (Potter, 1994).

The degree of preservation of Andean signatures along the Atlantic coast is primarily controlled by climate. The rivers draining the southern and central Andes flow through arid and semi-arid regions in which detritus undergoes limited chemical weathering (Potter, 1994). In contrast, detritus from northern Andes and drained to the Atlantic coast via the Amazon basin is derived from, and drains through, a humid and low-latitude area.

The Gondwana Sequence, with relatively low SiO_2, K_2O/Na_2O and strong "arc-type" chemistry, is compositionally most similar to the Andean association. The argillitic sediments of the Aileu Complex are more mature, siliceous and potassic, but nevertheless contain evidence of ultimately being derived from the east Pangaean arc. They are thus similar to the Transitional association.

Although the drainage network within northern Pangaea remains a matter of speculation, we believe it is reasonable to assume that it operated on a similar scale and yielded similarly consistent sediment associations as are observed presently in South America. If this is correct, we suggest that the distinctly different geochemical and isotopic character observed for the rocks of the Aileu Complex and Gondwana Sequence implies that these rocks were likely sourced from different sections of the Pangaean arc, transported along distinct drainage networks, and deposited in spatially separated basins. We cannot say how widely separated these basins were, although by comparison with the spacing of the outlets of the main drainage systems in South America and the very broad distribution of the main sediment types, we suggest that the distances could be significant (up to 10^3 km?).

6.3. Geodynamic implications

If the scenario presented above is correct, then the conclusion that the Aileu Complex represents the deep-water lateral equivalents of the Gondwana Sequence (Charlton et al., 2002; Keep and Haig, 2010) is unlikely to be correct. Instead we would argue that the current proximity of the Gondwana and Aileu sequences is tectonic, an inference broadly consistent the conclusions of Audley-Charles (1968), Carter et al. (1976), Barber et al. (1977) and Ely et al. (2014). However, a number of these studies also implied a northern Sundaland provenance for the Aileu Complex, a point we dispute given the consistent detrital zircon age spectra observed for both the Gondwana and Aileu sequences.

Given the Gondwana Sequence is in situ relative to comparable strata on the Australian Northwest Shelf (Audley-Charles, 1966), we infer that the deposition of the Aileu Complex occurred to the north of their present position of Timor. Similar to Charlton (2001) we postulate the existence of a Permo-Triassic seaway, the Banda Embayment, north and northeast of Timor (Figs. 10 and 11). We do not know the dimensions of this seaway although argue it was in this seaway that the protoliths of the Aileu Complex were likely deposited. Although the Maubisse Formation was deposited under shallow water conditions (Davydov et al., 2013), the bulk of the Aileu Complex is defined by a monotonous sequence of shale and mudstone that likely reflect a deep-water depositional environment. On this basis we speculate that at least parts of this seaway may have been underlain by oceanic crust.

The tectonic contact between the Gondwana Sequence and the Aileu Complex is defined by the Laclo Fault. This structure is a steeply-dipping and tectonically late feature (Grady, 1975; Duffy

et al., 2013) and, although the throw on this structure is likely to be significant, it does not necessarily accommodate all of the shortening required to juxtapose the rocks of the Aileu Complex against those of the Gondwana Sequence. This we believe is partly accommodated within the Aileu Complex itself and occurred during the Miocene as the Indo-Australian plate progressively converged with the Banda Arc.

Acknowledgements

SDB, RIL and LGS gratefully acknowledge the support our Timorese colleagues Lytha Argentina de Jesus Candido, José Fernandes Pinto, Neilton Raimundo Fernandes Xavier and particularly Joao (Jhony) Edmundo dos Reis for support and camaraderie during our field campaigns. The project was funded from ARC Discovery grant DP140104056 awarded to Mike Sandiford. The authors also acknowledge the efforts of Drs. Inga Sevastjanova and Timothy Charlton, whose review comments were of great help in crafting the final version of this manuscript.

References

Abbott, M.J., Chamalaun, F.H., 1981. Geochronology of some Banda arc volcanics. In: Wirosuyono, S. (Ed.), The Geology and Tectonics of Eastern Indonesia. Geological Research and Development Centre, Special Publication, pp. 253–271.

Allen, C.M., Williams, I.S., Stephens, C.J., Fielding, C.R., 1998. Granite genesis and basin formation in an extensional setting: the magmatic history of the northernmost New England Orogen. Aust. J. Earth Sci. 45, 875–888.

Audley-Charles, M.G., 2011. Tectonic post-collision processes in Timor. In: Hall, R., Cottam, M.A., Wilson, M.E.J. (Eds.), The SE Asian Gateway: History and Tectonics of the Australia-Asia Collision, vol. 335. Geological Society, London, Special Publications, pp. 241–266.

Audley-Charles, M.G., 2004. Ocean trench blocked and obliterated by Banda forearc collision with Australian proximal continental slope. Tectonophysics 389, 65–79.

Audley-Charles, M.G., 1968. The geology of Portuguese Timor. Geological Society, London, Memoir 4, 1–75.

Audley-Charles, M.G., 1966. Mesozoic palaeogeography of Australasia. Palaeogeogr. Palaeoclimatol. Palaeoecol. 2, 1–25.

Barber, A.J., Audley-Charles, M.G., 1976. The significance of the metamorphic rocks of Timor in the development of the Banda Arc, eastern Indondesia. Tectonophysics 30, 119–128.

Barber, A.J., Audley-Charles, M.G., Carter, D.J., 1977. Thrust tectonics in Timor. J. Geol. Soc. Aust. 24, 51–62.

Berry, R., Thompson, J., Meffre, S., Goemann, K., 2016. U–Th–Pb monazite dating and the timing of arc–continent collision in East Timor. Aust. J. Earth Sci. 63, 367–377.

Berry, R.F., 1981. Petrology of the Hili Manu lherzolite, East Timor. J. Geol. Soc. Aust. 28, 453–469.

Berry, R.F., Grady, A.E., 1981. Deformation and metamorphism of the Aileu Formation, north coast, East Timor and its tectonic significance. J. Struct. Geol. 3, 143–167.

Berry, R.F., Jenner, G.A., 1982. Basalt geochemistry as a test of the tectonic models of Timor. J. Geol. Soc., London 139, 593–604.

Berry, R.F., McDougall, I., 1986. Interpretation of $^{40}Ar/^{39}Ar$ and K/Ar dating evidence from the Aileu Formation, East Timor, Indonesia. Chem. Geol. 59, 43–58.

Betts, B.G., Giles, D., Mark, G., Lister, G.S., Goleby, B.R., Aillères, L., 2006. Synthesis of the Proterozoic evolution of the Mt Isa Inlier. Aust. J. Earth Sci. 53, 187–211.

Bhatia, M.R., 1983. Plate tectonics and geochemical composition of sandstones. J. Geol. 91, 611–627.

Bhatia, M.R., Crook, K.A.W., 1986. Trace element characteristics of graywackes and tectonic setting discrimination of sedimentary basins. Contrib. Miner. Petrol. 92, 181–193.

Bird, P.R., Cook, S.E., 1991. Permo-Triassic successions of the Kekneno area, West Timor: implications for palaeogeography and basin evolution. J. SE Asian Earth Sci. 6, 359–371.

Black, L.P., Kamo, S.L., Allen, C.M., Davis, D.W., Aleinikoff, J.N., Valley, J.W., Mundil, R., Campbell, I.H., Korsch, R.J., Williams, I.S., Foudoulis, C., 2004. Improved $^{206}Pb/^{238}U$ microprobe geochronology by the monitoring of a trace-element related matrix effect; SHRIMP, ID–TIMS, ELA–ICP–MS and oxygen isotope documentation for a series of zircon standards. Chem. Geol. 205, 115–140.

Black, L.P., McCulloch, M.T., 1990. Isotopic evidence for the dependence of recurrent felsic magmatism on new crust formation: an example from the Georgetown region of northeastern Australia. Geochem. Cosmochim. Acta 54, 183–196.

Black, L.P., Withnall, I.W., Gregory, P., Oversby, B.S., Bain, J.C.H., 2005. U-Pb zircon ages from leucogneiss in the Etheridge Group and their significance for the early history of the Georgetown region, north Queensland. Aust. J. Earth Sci. 52, 385–401.

Blewett, R.S., Black, L.P., Sun, S.-S., Hutton, L.J., Bain, J.C.H., 1998. U-Pb zircon and Sm-Nd geochronology of the Mesoproterozoic of north Queensland: implications and for Rodinia and connection with the Belt supergroup of North America. Precambr. Res. 89, 101–127.

Boger, S.D., 2011. Antarctica—before and after Gondwana. Gondwana Res. 19, 335–371.

Boger, S.D., Miller, J.M., 2004. Terminal suturing of Gondwana and the onset of the Ross-Delamerian Orogeny: the cause and effect of an Early Cambrian reconfiguration of plate motions. Earth Planet. Sci. Lett. 219, 35–48.

Brunnschweiler, R.O., 1978. Notes on the geology of eastern Timor. BMR Bull. Aust. Geol. Geophys. 192, 9–18.

Bryan, S.E., Allen, C.M., Holcombe, R.J., Fielding, C.R., 2004. U-Pb zircon geochronology of late Devonian to early Carboniferous extension-related silicic volcanism in the northern New England Fold Belt. Aust. J. Earth Sci. 51, 645–664.

Cande, S.C., Mutter, J.C., 1982. A revised identification of the oldest sea-floor spreading anomalies between Australia and Antarctica. Earth Planat. Sci. Lett. 58, 151–160.

Caprarelli, G., Leitch, E.C., 1998. Magmatic changes during the stabilisation of a cordilleran fold belt: the Late Carboniferous-Triassic igneous history of eastern New South Wales, Australia. Lithos 45, 413–430.

Carter, D.J., Audley-Charles, M.G., Barber, A.J., 1976. Stratigraphical analysis of island arc-continental margin collision in eastern Indonesia. J. Geol. Soc., London 132, 179–198.

Cawood, P.A., 2005. Terra Austaris Orogen: Rodinia breakup and the development of the Pacific and Iapetus margins of Gondwana during the Neoproterozoic and Paleozoic. Earth-Sci. Rev. 69, 249–279.

Cawood, P.A., Buchan, C., 2007. Linking accretionary orogenesis with supercontinent assembly. Earth-Sci. Rev. 82, 217–256.

Cawood, P.A., Hawkesworth, C.J., Dhuime, B., 2012. Detrital zircon record and tectonic setting. Geology 40, 875–878.

Cawood, P.A., Leitch, E.C., Merle, R.E., Nemchin, A.A., 2011. Orogenesis without collision: stabilizing the Terra Australis accretionary orogen, eastern Australia. Geol. Soc. Am. Bull. 123, 2240–2255.

Champion, D.C., Bultitude, R.J., 2013. The geochemical and Sr–Nd isotopic characteristics of Paleozoic fractionated S-types granites of north Queensland: implications for S-type granite petrogenesis. Lithos 162–163, 37–56.

Charlton, T.R., 2001. Permo-Triassic evolution of Gondwanan eastern Indonesia, and the final Mesozoic separation of SE Asia from Australia. J. Asian Earth Sci. 19, 595–617.

Charlton, T.R., 2002. The structural setting and tectonic significance of the Lolotoi, Laclubar and Aileu metamorphic massifs, East Timor. J. Asian Earth Sci. 20, 851–865.

Charlton, T.R., Barber, A.J., Harris, R.A., Barkham, S.T., Bird, P.R., Archbold, N.W., Morris, N.J., Nicoll, R.S., Owen, H.G., Owens, R.M., Sorauf, J.E., Taylor, P.D., Webster, G.D., Whittaker, J.E., 2002. The Permian of Timor: stratigraphy, paleaontology and palaeogeography. J. Asian Earth Sci. 20, 719–774.

Charlton, T.R., Barber, A.J., McGowan, A.J., Nicoll, R.S., Ronievicz, E., Cook, S.E., Barkham, S.T., Bird, P.R., 2009. The Triassic of Timor: lithostratigraphy, chronostratigraphy and palaeogeography. J. Asian Earth Sci. 36, 341–363.

Charlton, T.R., Wall, D., 1994. New biostratigraphie results from the Kolbano area, southern West Timor: implications for the Mesozoic-Tertiary stratigraphy of Timor. J. SE Asian Earth Sci. 9, 113–122.

Claoué-Long, J., Edgoose, C., Worden, K., 2008b. A correlation of Aileron Province stratigraphy in central Australia. Precambr. Res. 166, 230–245.

Claoué-Long, J., Maidment, D.W., Donnellan, N., 2008a. Stratigraphic timing constraints in the Davenport Province, central Australia: A basis for Palaeoproterozoic correlations. Precambr. Res. 166, 204–218.

Crowhurst, P.V., Maas, R., Hill, K.C., Foster, D.A., Fanning, C.M., 2004. Isotopic constraints on crustal architecture and Permo-Triassic tectonics in New Guinea: possible links with eastern Australia. Aust. J. Earth Sci. 51, 107–122.

Davydov, V.I., Haig, D.W., McCartain, E., 2013. A latest Carboniferous warming spike recorded by a fusulinid-rich bioherm in Timor Leste: implications for East Gondwana deglaciation. Palaeogeogr. Palaeoclimatol. Palaeoecol. 376, 22–38.

Dickinson, W.R., Beard, L.S., Brakenridge, G.R., Erjavec, J.L., Ferguson, R.C., Inman, K. F., Knepp, R.A., Lindberg, F.A., Ryberg, P.T., 1983. Provenance of North American Phanerozoic sandstones in relation to tectonic setting. Geol. Soc. Am. Bull. 94, 222–235.

Dinis, P.A., Tassinari, C., Cabral Pinto, M.M.S., 2013. Geochemistry and detrital geochronology of stream sediments from East Timor: implications for the origin of source units. Aust. J. Earth Sci. 60, 509–519.

Duffy, B., Quigley, M., Harris, R., Ring, U., 2013. Arc-parallel extrusion of the Timor sector of the Banda arc-continent collision. Tectonics 32, 641–660.

Eggins, S.M., Woodhead, J.D., Kinsley, L.P.J., Mortimer, G.E., Sylvester, P., McCulloch, M.T., Hergt, J.M., Handler, M.R., 1997. A simple method for the precise determination of ⩾40 trace elements in geological samples by ICPMS using enriched isotope internal standardisation. Chem. Geol. 134, 311–326.

Ely, K.S., Sandiford, M., Hawke, M.L., Phillips, D., Quigley, M., dos Reis, J.E., 2011. Evolution of Ataúro Island: temporal constraints on subduction processes beneath the Wetar zone, Banda Arc. J. Asian Earth Sci. 41, 477–493.

Ely, K.S., Sandiford, M., Phillips, D., Boger, S.D., 2014. Detrital zircon U-Pb and 40Ar/39Ar hornblende ages from the Aileu Complex, Timor-Leste: provenance and metamorphic cooling history. J. Geol. Soc., London 171, 299–309.

Eyles, N., Mory, A.J., Backhouse, J., 2002. Carboniferous-Permian palynostratigraphy of west Australian marine rift basins: resolving tectonic and eustatic controls

during Gondwanan glaciations. Palaeogeogr. Palaeoclimatol. Palaeoecol. 184, 305–319.
Fergusson, C.L., Carr, P.F., Fanning, C.M., Green, T.J., 2001. Proterozoic-Cambrian detrital zircon and monazite ages from the Anakie Inlier, central Queensland: Grenville and Pacific-Gondwana signatures. Aust. J. Earth Sci. 48, 857–866.
Fergusson, C.L., Henderson, R.A., Fanning, C.M., Withnall, I.W., 2007a. Detrital zircon ages in Neoproterozoic to Ordovician siliciclastic rocks, northeastern Australia: implications for the tectonic history of the East Gondwana continental margin. J. Geol. Soc. London 164, 215–225.
Fergusson, C.L., Henderson, R.A., Withnall, I.W., Fanning, C.M., Phillips, D., 2007b. Structural, metamorphic, and geochronological constraints on alternating compression and extension in the Early Paleozoic Gondwanan Pacific margin, northeastern Australia. Tectonics 26, TC3008. http://dx.doi.org/10.1029/2006TC001979.
Foden, J., Elburg, M.A., Dougherty-Page, J., Burtt, A., 2006. The timing and duration of the Delamerian Orogeny: correlation with the Ross Orogen and implications for Gondwana assembly. J. Geol. 114, 189–210.
Genrich, J., Bock, Y., McCaffrey, R., Calais, E., Stevenc, C.W., Subarya, C., 1996. Accretion of the southern Banda arc to the Australian plate margin determined by Global Positioning System measurements. Tectonics 15, 288–295.
Giles, D., Nutman, A.P., 2002. SHRIMP U-Pb monazite dating of 1600–1580 Ma amphibolite facies metamorphism in the southeastern Mt Isa Block, Australia. Aust. J. Earth Sci. 49, 455–465.
Gleadow, A.J.W., Kohn, B.P., Brown, R.W., O'Sullivan, P.B., Raza, A., 2002. Fission track thermotectonic imaging of the Australian continent. Tectonophysics 349, 4–21.
Goldstein, S.L., O'Nions, R.K., Keith, R., Hamilton, P.J., 1984. A Sm-Nd isotopic study of atmospheric dusts and particulates from major river systems. Earth Planat. Sci. Lett. 70, 221–236.
Grady, A.E., 1975. A reinvestigation of thrusting in Portugese Timor. J. Geol. Soc. Aust. 22, 223–227.
Grunau, H.R., 1953. Geologie von Portugiesisch Ost-Timor. Eine kurze Übersicht. Eclogae Geologicae Helvetiae 46, 29–37.
Haig, D.W., 2012. Palaeobathymetric gradients across Timor during 5.7–3.3 Ma (latest Miocene–Pliocene) and implications for collision uplift. Palaeogeogr. Palaeoclimatol. Palaeoecol. 331–332, 50–59.
Haig, D.W., McCartain, E., 2007. Carbonate pelagites in the post-Gondwana succession (Cretaceous – Neogene) of East Timor. Aust. J. Earth Sci. 54, 875–897.
Haig, D.W., McCartain, E., 2012. Intraspecific variation in Triassic Ophthalmidiid Foraminifera from Timor. Rev. Micropaléontol. 55, 39–52.
Haig, D.W., McCartain, E., Mory, A.J., Borges, G., Davydov, V.I., Dixon, M., Ernst, A., Groflin, S., Håkansson, E., Keep, M., Dos Santos, Z., Shi, G.R., Soares, J., 2014. Postglacial Early Permian (late Sakmarian–early Artinskian) shallow-marine carbonate deposition along a 2000 km transect from Timor to west Australia. Palaeogeogr. Palaeoclimatol. Palaeoecol. 409, 180–204.
Hall, R., 2002. Cenozoic geological and plate tectonic evolution of SE Asia and the SW Pacific: computer-based reconstructions, model and animations. J. Asian Earth Sci. 20, 353–431.
Hall, R., 2012. Late Jurassic-Cenozoic reconstructions of the Indonesian region and the Indian Ocean. Tectonophysics 570–571, 1–41.
Harris, R., 2006. Rise and fall of the Eastern Great Indonesian arc recorded by the assembly, dispersion and accretion of the Banda Terrane, Timor. Gondwana Res. 10, 207–231.
Harris, R., Kaiser, J., Hurford, A., Carter, A., 2000. Thermal history of Australian passive margin cover sequences accreted to Timor during Late Neogene arc-continent collision, Indonesia. J. Asian Earth Sci. 18, 47–69.
Harris, R.A., 1991. Temporal distribution of strain in the active Banda orogen: a reconciliation of rival hypotheses. J. SE Asian Earth Sci. 6, 373–386.
Harrowfield, M., Holgate, G.R., Wilson, C.J.L., McLoughlin, S., 2005. Tectonic significance of the Lambert graben, East Antarctica: reconstructing the Gondwanan rift. Geology 33, 197–200.
Hensel, H.-D., McCulloch, M.T., Chappell, B.W., 1985. The New England Batholith: constraints on its derivation from Nd and Sr isotopic studies of granitoids and country rocks. Geochem. Cosmochim. Acta 49, 369–384.
Hutton, L.J., Draper, J.J., Rienks, I.P., Withnall, I.W., Knutson, J., 1997. In: Bain, J.C.H., Draper, J.J. (Eds.), Charters Towers Region, North Queensland Geology. Australian Geological Survey Organisation Bulletin, pp. 165–224 (Chapter 6).
Jenkins, R.B., Landenberger, B., Collins, W.J., 2002. Late Palaeozoic retreating and advancing subduction boundary in the New England Fold Belt, New South Wales. Aust. J. Earth Sci. 49, 467–489.
Kaneko, Y., Maruyama, S., Kadarusman, A., Ota, T., Ishikawa, M., Tsujimori, T., Ishikawa, A., Okamoto, K., 2007. On-going orogeny in the outer-arc of the Timor-Tanimbar region, eastern Indonesia. Gondwana Res. 11, 218–233.
Keep, M., Haig, D.W., 2010. Deformation and exhumation in Timor: distinct stages of a young orogeny. Tectonophysics 483, 93–111.
Korsch, R.J., Totterdell, J.M., Cathro, D.L., Nicoll, M.G., 2009b. Early Permian East Australian Rift System. Aust. J. Earth Sci. 56, 381–400.
Korsch, R.J., Totterdell, J.M., Fomin, T., Nicoll, M.G., 2009a. Contractional structures and deformational events in the Bowen, Gunnedah and Surat Basins, eastern Australia. Aust. J. Earth Sci. 56, 477–499.
Koulali, A., Susilo, S., McCusky, S., Meilano, I., Cummins, P., Tregoning, P., Lister, G., Efendi, J., Syafi'i, M.A., 2016. Crustal strain partitioning and the associated earthquake hazard in the eastern Sunda-Banda Arc. Geophys. Res. Lett. 43, 1943–1949. http://dx.doi.org/10.1002/2016GL067941.
Kwon, C.W., Kim, S.W., Park, S.-I., Park, J., Oh, J.H., Kim, B.C., Koh, H.J., Cho, D.-L., 2014. Sedimentological characteristics and new detrital zircon SHRIMP U-Pb ages of the Babulu Formation in the Fohorem area, Timor-Leste. Aust. J. Earth Sci. 61, 865–880.
Lehner, B., Verdin, K., Jarvis, A., 2006. HydroSHEDS Technical Documentation. World Wildlife Fund US, Washington DC. Available at <http://hydrosheds.cr.usgs.gov>.
Maas, R., Grew, E.S., Carson, C.J., 2015. Isotopic constraints (Pb, Rb-Sr, Sm-Nd) on the sources of Early Cambrian pegmatites with boron and beryllium minerals in the Larseman Hills, Prydz Bay, Antarctica. Can. Mineral. 53, 249–272.
McLennan, S.M., Hemming, S., McDaniel, D.K., Hanson, G.N., 1993. Geochemical approaches to sedimentation, provenance, and tectonics. In: Johnsson, M.J., Basu, A. (Eds.), Processes Controlling the Composition of Clastic Sediments. Geological Society of America Special Paper 284, Boulder, Colorado.
McLennan, S.M., Taylor, S.R., 1991. Sedimentary rocks and crustal evolution: tectonic setting and seculat trends. J. Geol. 99, 1–21.
McLennan, S.M., Taylor, S.R., McCulloch, M.T., Maynard, J.B., 1990. Geochemical and Nd-Sr isotopic composition of deep-sea turbidites: crustal evolution and plate tectonic associations. Geochim. Cosmochem. Acta 54, 2015–2050.
Metcalfe, I., 2013b. Gondwana dispersion and Asian accretion: tectonic and palaeogeographic evolution of eastern Tethys. J. Asian Earth Sci. 66, 1–33.
Metcalfe, I., 2013a. Tectonic evolution of the Malay Peninsula. J. Asian Earth Sci. 76, 195–213.
Mortimer, N., Hauff, F., Calvert, A.T., 2008. Continuation of the New England Orogen, Australia, beneath the Queensland Plateau and Lord Howe Rise. Aust. J. Earth Sci. 55, 195–209.
Mory, A.J., Redfern, J., Martin, J.R., 2008. A review of Permian-Carboniferous glacial deposits in Western Australia. In: Fielding, C.R., Frank, T.D., Isbell, J.L. (Eds.), Resolving the late Paleozoic Ice Age in Time and Space. Geological Society of America Special Paper, pp. 29–40.
Muir, R.J., Ireland, T.R., Weaver, S.D., Bradshaw, J.D., Evans, J.A., Eby, G.N., Shelley, D., 1998. Geochronology and geochemistry of a Mesozoic magmatic arc system, Fiordland, New Zealand. J. Geol. Soc., London 155, 1037–1053.
Murgulov, V., Griffin, W.L., O'Reilly, S.Y., 2013. Carboniferous and Permian granites of the northern Tasman orogenic belt, Queensland, Australia: insights into petrogenesis and crustal evolution from an in situ zircon study. Int. J. Earth Sci. 102, 647–669.
Neumann, N.L., Southgate, P.N., Gibson, G.M., 2009. Defining unconformities in Proterozoic sedimentary basins using detrital geochronology and basin analysis—an example from the Mount Isa Inlier, Australia. Precambr. Res. 168, 149–166.
Neumann, N.L., Southgate, P.N., Gibson, G.M., McIntrye, A., 2006. New SHRIMP geochronology for the Western Fold Belt of the Mt Isa Inlier: developing a 1800–1650 Ma event framework. Aust. J. Earth Sci. 53, 1023–1039.
Nishiya, T., Watanabe, T., Yokoyama, K., Kuramoto, Y., 2003. New isotopic constraints on the age of the Halls Reward Metamorphics, North Queensland, Australia: delamerian metamorphic ages and Grenville detrital zircons. Gondwana Res. 6, 241–249.
Nugroho, H., Harris, R., Lestariya, A.W., Maruf, B., 2009. Plate boundary reorganization in the active Banda Arc–continent collision: insights from new GPS measurements. Tectonophysics 479, 52–65.
Offler, R., Foster, D.A., 2008. Timing and development of oroclines in the southern New England Orogen, New South Wales. Aust. J. Earth Sci. 55, 331–340.
Page, R.W., Sun, S.-S., 1998. Aspects of geochronology and crustal evolution in the Eastern Fold Belt, Mt Isa Inlier. Aust. J. Earth Sci. 45, 343–361.
Pankhurst, R.J., Vaughan, A.P.M., 2009. The tectonic context of the Early Palaeozoic southern margin of Gondwana. In: Bassett, M.G. (Ed.), Early Palaeozoic Peri-Gondwana Terranes: New Insights from Tectonics and Biogeography, vol. 325. Geological Society, London, Special Publications, pp. 171–176.
Park, S.-I., Kwon, S., Kim, S.W., 2014. Evidence for the Jurassic arc volcanism of the Lolotoi complex, Timor: tectonic implications. J. Asian Earth Sci. 95, 254–265.
Paton, C., Woodhead, J.D., Hellstrom, J.C., Hergt, J.M., Greig, A., Maas, R., 2010. Improved laser ablation U-Pb zircon geochronology through robust downhole fractionation correction. Geochem. Geophys. Geosyst. 11, Q0AA06.
Pin, C., Zalduegui, J.S., 1997. Sequential separation of light rare-earth elements, thorium and uranium by miniaturized extraction chromatography: application to isotopic analyses of silicate rocks. Anal. Chim. Acta 339, 79–89.
Potter, P.E., 1994. Modern sands of South America: composition, provenance and global significance. Geol. Rundsch. 83, 212–232.
Roberts, J., Claoué-Long, J., Foster, C.B., 1996. SHRIMP zircon dating of the Permian System of eastern Australia. Aust. J. Earth Sci. 43, 401–421.
Roberts, J., Claoue-Long, J., Jones, P.J., Foster, C.B., 1995. SHRIMP zircon age control of Gondwanan sequences in Late Carboniferous and Early Permian Australia. In: Dunay, R.E., Hailwood, E.A. (Eds.), Non-Biostratigraphical Methods of Dating and Correlation. Geological Society Special Publication, pp. 145–174.
Rösel, R., Zack, T., Boger, S.D., 2014. LA-ICP-MS U-Pb dating of detrital rutile and zircon from the Reynolds Range: a window into the Palaeoproterozoic tectonosedimentary evolution of the North Australian Craton. Precambr. Res. 255, 381–400.
Rosenbaum, G., Li, P., Rubatto, D., 2012. The contorted New England Orogen (eastern Australia): new evidence from U-Pb geochronology of early Permian granitoids. Tectonics, TC1006. http://dx.doi.org/10.1029/2011TC002960.
Roser, P.B., Korsch, R.J., 1986. Determination of tectonic setting of sandstone-mudstone suites using SiO_2 content and K_2O/Na_2O ratio. J. Geol. 94, 635–650.
Searle, M.P., Whitehouse, M.J., Robb, L.J., Ghani, A.A., Hutchinson, C.S., Sone, M., Ng, S.W.-P., Roselee, M.H., Chung, S.-L., Oliver, G.J.H., 2012. Tectonic evolution of the Sibumasu-Indochina terrane collision zone in Thailand and Malaysia: constraints from new U-Pb zircon chronology of SE Asian tin granitoids. J. Geol. Soc., London 169, 489–500.

Simons, W.J.F., Socquet, A., Vigny, C., Abbrosius, B.A.C., Haji Abu, S., Promthong, C., Subarya, C., Sarsito, D.A., Matheussen, S., Morgan, P., Spakman, W., 2007. A decade of GPS in Southeast Asia: resolving Sundaland motion and boundaries. J. Geophys. Res. 112, B06420. http://dx.doi.org/10.1029/2005JB003868.

Sircombe, K.N., Hazelton, M.L., 2004. Comparison of detrital zircon age distributions by kernel functional estimation. Sed. Geol. 171, 91–111.

Sláma, J., Košler, J., Condon, D.J., Crowley, J.L., Gerdes, A., Hanchar, J.M., Horstwood, M.S.A., Morris, G.A., Nasdala, L., Norberg, N., Schaltegger, U., Schoene, B., Tubrett, M.N., Whitehouse, M.J., 2008. Plešovice zircon—a new natural reference material for U-Pb and Hf isotopic microanalysis. Chem. Geol. 249, 1–35.

Spakman, W., Hall, R., 2010. Surface deformation and slab–mantle interaction during Banda arc subduction rollback. Nat. Geosci. 3, 562–566.

Spencer, C.J., Harris, R.A., Major, J.R., 2016. Provenance of Permian-Triassic Gondwana Sequence units accreted to the Banda Arc in the Timor region: constraints from zircon U-Pb and Hf isotopes. Gondwana Res. 38, 28–39.

Špičák, A., Matějkov, R., Vaněk, J., 2013. Seismic response to recent tectonic processes in the Banda Arc region. J. Asian Earth Sci. 64, 1–13.

Standley, C.E., Harris, R., 2009. Tectonic evolution of forearc nappes of the active Banda arc-continent collision: origin, age, metamorphic history and structure of the Lolotoi Complex, East Timor. Tectonophysics 479, 66–94.

Sun, S.S., McDonough, W.F., 1989. Chemical and isotopic systematics of ocean basalts: implications for mantle composition and processes. In: Saunders, A.D., Norry, M.J. (Eds.), Magmatism in Ocean Basins. Geological Society of London, Special Publications, London, pp. 313–345.

Tate, G.W., McQuarrie, N., Van Hinsbergen, D.J.J., Bakker, R.R., Harris, R., Willett, S., Reiners, P.W., Fellin, M.G., Ganerød, M., Zachariasse, W.J., 2014. Resolving spatial heterogeneities in exhumation and surface uplift in Timor-Leste: constraints on deformation processes in young orogens. Tectonics 33, 1089–1112. http://dx.doi.org/10.1002/2013TC003436.

Taylor, S.R., McLennan, S.M., 1985. The Continental Crust: Its Composition and Evolution. Blackwell, Oxford, p. 312.

Tulloch, A.J., Ramezani, J., Kimbrough, D.L., Faure, K., Allibone, A.H., 2009. U-Pb geochronology of mid-Paleozoic plutonism in western New Zealand: implications for S-type granite generation and growth of the east Gondwana margin. Geol. Soc. Am. Bull. 121, 1236–1261.

Van Wyck, N., Williams, I.S., 2002. Age and provenance of basement metasediments from the Kubor and Bena Bena Blocks, central Highlands, Papua New Guinea: constraints on the tectonic evolution of the northern Australian cratonic margin. Aust. J. Earth Sci. 49, 565–577.

Verma, S.P., Armstrong-Altrin, J.S., 2013. New multi-dimensional diagrams for tectonic discrimination of siliciclastic sediments and their application to Precambrian basins. Chem. Geol. 335, 117–133.

Vermeesch, P., 2004. How many grains are needed for a provenance study? Earth Planat. Sci. Lett. 224, 441–451.

Vermeesch, P., 2012. On the visualisation of detrital age distributions. Chem. Geol. 312–313, 190–194.

Wiedenbeck, M., Hanchar, J.M., Peck, W.H., Sylvester, P., Valley, J., Whitehouse, M., Kronz, A., Morishita, Y., Nasdala, L., Fiebig, J., Franchi, I., Girard, J.-P.G., Greenwood, R.C., Hinton, R., Kita, N., Mason, P.R.D., Norman, M., Ogasawara, M., Piccoli, P.M., Rhede, D., Satoh, H., Schulz-Dobrick, B., Skår, Ø., Spicuzza, M.J., Terada, K., Tindle, A., Togashi, S., Vennemann, T., Xie, Q., Zheng, Y.-F., 2004. Further characterisation of the 91500 zircon crystal. Geostandard Geoanal. Res. 28, 9–39.

Withnall, I.W., Black, L.P., Harvey, K.J., 1991. Geology and geochronology of the Balcooma area: Part of an Early Palaeozoic magmatic belt in North Queensland. Aust. J. Earth Sci. 38, 15–29.

Woodhead, J.D., 2002. A simple method for obtaining highly accurate Pb isotope data by MC-ICP-MS. J. Anal. At. Spectrom. 17, 1381–1385.

Zimmermann, S., Hall, R., 2016. Provenance of Triassic and Jurassic sandstones in the Banda Arc: Petrography, heavy minerals and zircon geochronology. Gondwana Res. 37, 1–19.